(T761E) or IBMPFD-VCPs and immunoprecipitated FLAG-tagged VCPs with anti-FLAG M2 affinity gel. Coprecipitated endogenous Npl4, Ufd1, p47 and ubiquitinated proteins were examined by Western blot analysis. Npl4 and Ufd1 were coprecipitated more potently with all tested IBMPFD-VCPs than with wt-VCP (Fig. 5A). In contrast, the amounts of p47 precipitated with all IBMPFD-VCPs were only marginally higher than those precipitated with wt-VCP (Fig. 5A). Furthermore, polyubiquitinated proteins were more robustly bound to all tested IBMPFD-VCPs when compared with wt-VCP (Fig. 5A). These results suggest that the binding abilities to these cofactors, especially to Npl4 and Ufd1, were elevated in IBMPFD-VCPs. In contrast, wt-VCP and VCP(T761E) behave indistinguishably (Fig. 5B), indicating that the cofactor-binding abilities do not directly link to the ATPase activities. Knockdown of Npl4 and Ufd1 reduced the amount of coprecipitated polyubiquitinated proteins by IBMPFD-VCPs, as in VCP(R155C) and VCP(A232E) (Fig. 5C). These results suggest that binding of polyubiquitinated

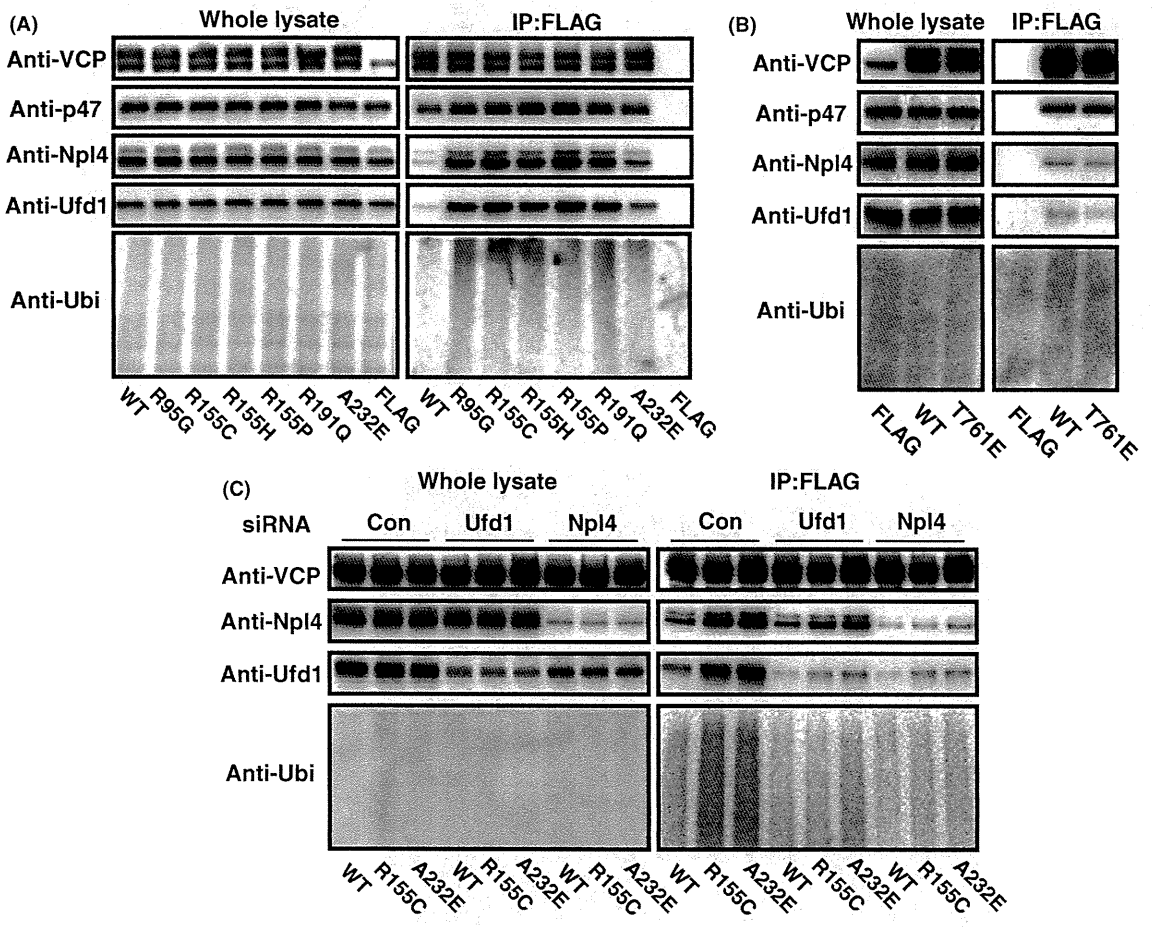

Figure 5 Enhanced cofactor-binding abilities of IBMPFD-VCPs. (A) Western blot analysis of VCP cofactors coimmunoprecipitated with FLAG-tagged wt-VCP or IBMPFD-VCPs. Immunoprecipitated VCP cofactors such as p47 (anti-p47), Npl4 (anti-Npl4) and Ufd1 (anti-Ufd1) or ubiquitinated proteins (anti-Ubi) were detected using specific antibodies (right panels). The whole cell lysates were also analyzed (left panels). (B) Western blot analysis of VCP cofactors coimmunoprecipitated with FLAG-tagged wt-VCP or VCP(T761E), as described in (A). (C) Western blot analysis of VCP cofactors coimmunoprecipitated with FLAG-tagged VCPs in cofactor knockdown cells. HEK293 cells were transfected with control siRNA, Ufd1 siRNA (216), Npl4 siRNA (679). Three days after transfection, FLAG-tagged VCPs were expressed for 1 day and analyzed as described in (A). IBMPFD, inclusion body myopathy associated with Paget disease of bone and frontotemporal dementia; VCP, valosin-containing protein.

proteins to IBMPFD-VCPs were enhanced with a help of Npl4 and Ufd1.

Phenotypes of IBMPFD-VCPs in *Drosophila* models

Finally, we examined the *in vivo* phenotypes of IBMPFD-VCPs by expressing IBMPFD-VCPs in fly eyes. Contrary to ter94 (*Drosophila* VCP) (Higashiyama *et al.* 2002), wt-VCP and all tested IBMPFD-VCPs as well as VCP(T761E) did not induce eye degenerations by themselves (Fig. 6A). However, by expression of wt-VCP with polyglutamines, the eye degenerations were mitigated (Koike *et al.* 2010). In contrast, VCP(T761E), VCP(R155H), VCP(R155P) and VCP(A232E), which all possessed elevated ATPase activities (Fig. 4C,D), worsened the polyglutamine-induced eye degenerations (Fig. 6A). Surprisingly, we

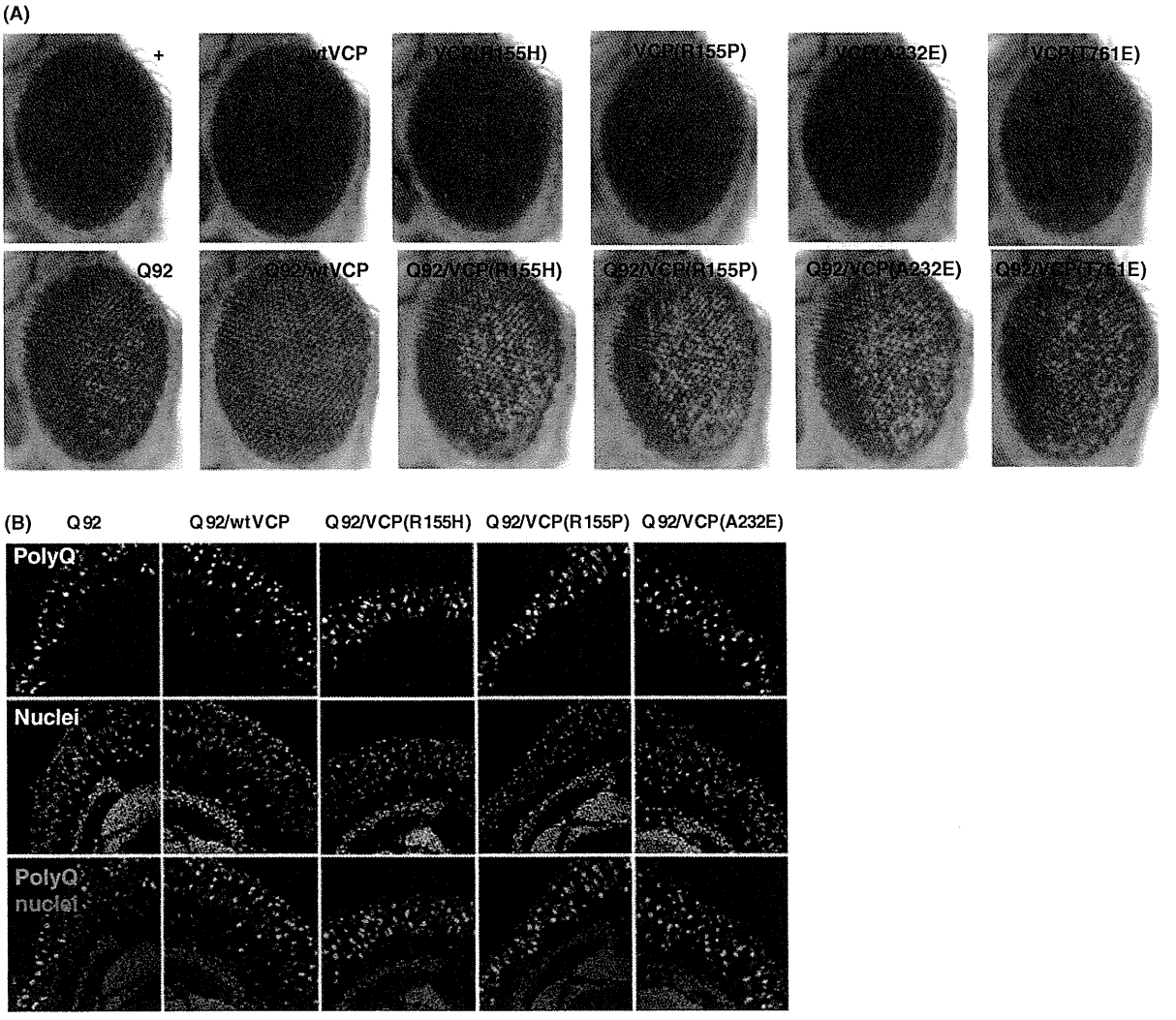

Figure 6 Effects of wt-VCP and mutant VCPs on eye degeneration and polyglutamine aggregate formation in *Drosophila*. (A) Light microphotographs of the compound eye from 5-day-old flies. wt-VCP and IBMPFD-VCPs and VCP(T761E) were expressed alone and together with FLAG-Q92 in *Drosophila* compound eyes (Higashiyama *et al.* 2002). (B) Confocal images of cryosections from 5-day-old fly heads. FLAG-Q92 was detected with anti-FLAG M5 antibody, and nuclei were stained with TOTO-3. In the overlay images, green indicates FLAG-Q92 and magenta indicates the nuclei. Genotypes of the flies are shown in the panels (A) or above the panels (B). IBMPFD, inclusion body myopathy associated with Paget disease of bone and frontotemporal dementia; VCP, valosin-containing protein.

could not observe apparent differences in sizes and frequencies of polyglutamine aggregates between eyes expressing wt-VCP and IBMPFD-VCPs (Fig. 6B).

Discussion

VCP colocalizes with abnormal protein aggregates observed in various neurodegenerative disorders (Hirabayashi *et al.* 2001; Mizuno *et al.* 2003; Ishigaki *et al.* 2004). We have recently showed that VCP functions as an aggregate-formase and/or as an aggregate-unfoldase (Kobayashi *et al.* 2007), but precise conditions or mechanisms that regulate either activity have remained to be clarified. In this study, we elucidated certain aspects of the aggregate-forming activity. We expressed VCP-GFP in the cells, treated the cells with proteasome inhibitors and then traced GFP signals via fluorescent time-lapse microscopy (Fig. 1B). VCP first appeared to bind abnormal proteins and formed several small aggregates throughout the cells and then carried them to the aggresome, vimentin-positive large aggregates (Johnston *et al.* 1998). Consistent with this, forced localization of VCP in the nucleus, by tagging NLS, created polyglutamine aggregates more frequently in the nucleus (Fig. 2). Although VCP usually colocalized with cytoplasmic polyglutamine aggregates, such colocalization was apparently destroyed in the nucleus in this cell culture experiment, suggesting that in the nucleus there may exist a protein(s) with affinity for abnormal proteins such as expanded polyglutamine much higher than that of VCP. VCP may hand out abnormal proteins to such a protein(s) in the nucleus. This possibility remains to be tested.

VCP colocalization with aggregates has been also observed in pathological samples of patients suffering from IBMPFD (Watts *et al.* 2004; Schröder *et al.* 2005). Given that VCP functions as an aggregate-formase or as an aggregate-unfoldase (Kobayashi *et al.* 2007), such colocalization is because of either elevated aggregate-formase activities or decreased aggregate-unfoldase activities in IBMPFD-VCPs. We indeed found that aggregate-forming activities were enhanced in IBMPFD-VCPs (Fig. 4A,B). This observation suggests that IBMPFD-VCPs make aggregates more efficiently than wt-VCP.

Biochemically, all immunopurified IBMPFD-VCPs showed significantly elevated ATPase activities, when compared with wt-VCP (Fig. 4C,D). Previously, it has been shown that ATPase activity of VCP(R155H) is normal by other group (Weihl *et al.* 2006). Indeed, elevation of the ATPase activities of VCP(R155H) was the lower than that of VCP(A232E), but was significantly higher than that of wild-type VCP in two different methods in our experiments (Fig. 4C,D). In addition, immunoprecipitation experiments demonstrated that IBMPFD-VCPs possessed elevated affinities for Ufd1 and Npl4, as well as for polyubiquitinated proteins (Fig. 5A). Either Ufd1 siRNA or Npl4 siRNA mostly abolished enhancement of IBMPFD-VCPs to bind the other partners and polyubiquitinated proteins (Fig. 5C). These results clearly showed that IBMPFD-VCPs, Ufd1 and Npl4 do bind polyubiquitinated proteins cooperatively. Consistent with this, the formation of polyglutamine aggregates was inhibited by VCP siRNA, Npl4 siRNA or Ufd1 siRNAs (Fig. 3). These results indicate that VCP, Ufd1 and Npl4, as a complex, were involved in forming abnormal protein aggregates.

The data presented in this study, collectively, indicated that IBMPFD-VCPs possess elevated ATPase activities (Fig. 4C,D) and enhanced abilities in binding to the cofactors, especially to Npl4 and Ufd1 as well as to polyubiquitinated proteins (Fig. 5A), leading to acceleration of abnormal protein aggregate formation in mammalian cells. Thus, we expected IBMPFD-VCPs to induce more polyglutamine aggregates in our fly models of polyglutamine disease, leading to more severe eye degenerations. This expectation was partly the case; co-expression of IBMPFD-VCPs enhanced polyglutamine-induced eye degenerations (Fig. 6A). But contrary to our expectation, levels of polyglutamine aggregates were not apparently affected by IBMPFD-VCPs in *Drosophila* eyes (Fig. 6B). This might be because of different nature of Ufd1 and Npl4 between mammals and *Drosophila*. Namely, IBMPFD-VCPs may possess elevated affinities for human Ufd1 and Npl4 but not for *Drosophila* Ufd1 or Npl4. This possibility remains to be tested.

Along with IBMPFD-VCPs, VCP(T761E) also enhanced the eye degenerations in a very similar way (Fig. 6A). These results indicated that in *Drosophila*, elevated ATPase activities of VCP are coupled profoundly with eye degenerations, but such pathogenic effects were only manifested in the presence of abnormal proteins such as polyglutamines, which is reminiscent of aging and could provide an explanation as to why IBMPFD is a late-onset disease. It is, however, currently unknown that similar situations are indeed applicable to the pathogenesis in human IBMPFD and its related disorders. But it is notable that among IBMPFD-VCPs, VCP(A232E) showed the highest ATPase activities (Fig. 4C,D), and it represented the severest clinical phenotypes (Watts *et al.* 2004). Further studies on VCP functions will

elucidate more detailed molecular mechanisms of human disorders with neurodegenerations, myopathy and bone disorders (Custer *et al.* 2010; Koike *et al.* 2010) and will lead to novel therapeutic hints on such currently noncurable disorders.

Experimental procedures

siRNAs

We tested three sets of siRNA for each mRNA and obtained essentially same results. Used siRNAs (VCP, Ufd1, Npl4, and p47 siRNAs) sequences were listed in Table S1 in supplement materials. All siRNA for the target proteins manifested essentially same phenotypes.

Antibodies and plasmids

The affinity-purified rabbit polyclonal anti-VCP, anti-p47, anti-Npl4 and anti-Ufd1 antibodies were developed previously (Noguchi *et al.* 2005). The following antibodies used in this study were purchased: mouse monoclonal anti-ubiquitin (Chemicon); mouse monoclonal anti-FLAG M5 (Sigma); mouse monoclonal anti-actin (Chemicon); rat monoclonal anti-GFP (Nacalai Tesque); mouse monoclonal anti-vimentin (V9) (Santa Cruz Biotechnology, Inc.); Alexa Fluor 488 goat anti-rat IgG and Alexa Fluor 594 goat anti-mouse IgG (Molecular Probes); donkey polyclonal anti-mouse IgG-HRP and anti-rabbit IgG-HRP (Amersham Biosciences). IBMPFD-associated VCP mutants expressing plasmid were constructed by site-directed mutagenesis. Plasmids encoding GFP-fused wt-VCP and various VCP mutants were constructed in pEGFP-N vector (Clontech).

Time-lapse imaging

For time-lapse imaging, HEK293 cells were seeded onto collagen-coated 35 -mm glass bottom dish (IWAKI). After attachment, cells were transfected with VCP-GFP expressing plasmids. Twelve hours after transfection, cells were treated with 1 μM MG132. After this treatment, cell morphologies and GFP signals were recorded during 24 h using an inverted fluorescence microscopy (Axiovert 200M; Carl Zeiss). Image analysis and processing were performed via the ZEISS AXIOVISION 4.5 software.

Quantification of aggregate formation

Approximately more than 500 randomly selected FLAG/GFP-positive cells per each sample were counted for aggregate formation by fluorescence microscopy (Axiovert 200M). Cells were scored positive if they contained one or several visible aggregates either in the cytoplasm or in the nucleus. Frequency of aggregate formation in transfected cells represents the percentage of the FLAG/GFP-positive cells that contained visible aggregates inside the cell.

Immunoprecipitation

For immunoprecipitation, HEK293 cells were transfected with a FLAG-VCP expression plasmid. One day after transfection, cells were harvested and lysed in 0.1% Triton lysis buffer. Each sample was mixed with anti-FLAG M2 Affinity Gel (Sigma), and stirred at 4 °C overnight. FLAG-VCP was eluted with FLAG-peptide (Sigma).

Measurement of ATPase activities

In this report, we measured ATPase activities of wt-VCP and various VCP mutants both by the molybdate assay and by the NADH-coupled assay. The procedures of both assays were as described previously (Kobayashi *et al.* 2002; Noguchi *et al.* 2005; Mori-Konya *et al.* 2009). In the molybdate assay, 500 ng of VCP protein was incubated in 20 μL of the ATPase assay buffer (20 mM HEPES (pH 7.4), 50 mM KCl, 5 mM $MgCl_2$) with 100 μM [γ-^{32}P]ATP (18.5GBq/mmol) (PerkinElmer) at 37 °C for 10 min. After incubation, the reaction was quenched by the addition of 200 μL of 7% ice-cold TCA solution with 1 mM K_2HPO_4, and then 50 μL of solution A (3.75% ammonium molybdate, 0.02 M silicotungstic acid in 3 N H_2SO_4) and 300 μL of *n*-butyl acetate were added to the reaction. The samples were mixed well and centrifuged at 12 000 ×***g*** for 1 min. Then, 200 μL aliquots from the upper organic phases were taken, and their radioactivity was determined with a liquid scintillation counter for β-radiation, which determined the amounts of ^{32}P released. In the NADH-coupled assay, several different amounts of VCP proteins (1, 2, 5, and 10 μg) were preincubated at 37 °C for 10 min and then incubated with the ATPase assay buffer (50 mM Tris–HCl (pH 9.0), 150 mM NaCl, 2 mM $MgSO_4$), 3 mM phosphoenol pyruvate, 1 mM ATP, 0.25 mM NADH, 1.0 unit of pyruvate kinase and 1.5 units of lactate dehydrogenase. The absorbance of NADH was measured at 340 nm for 20 min at 37 °C.

Drosophila strain and genetics

Fly culture and crosses were performed at 25 °C on standard food. To generate UAS-mutant VCP flies, cDNAs of each mutant VCP were subcloned into BglII-NotI site of pUAST vector. Transgenic flies were generated by standard protocols. Several independent lines were established from each construct. GMR-Gal4 and GMR-FlagQ92 were described previously (Higashiyama *et al.* 2002).

Immunohistochemistry

Eye sections were incubated in 1 mg/mL RNase/PBS for 30 min at 37 °C and stained with 1 μM TOTO-3 (Invitrogen) at room temperature (RT) for 2 h. After TOTO-3 staining,

sections were incubated with anti-FLAG monoclonal antibody M5 (Sigma) at 1 : 1000 dilution in 5% skim milk/PBT at RT for 2 h. Then, sections were incubated with Alexa 488-labeled anti-mouse IgG antibody at 1 : 500 dilution in 5% skim milk/PBT at RT for 30 min and were analyzed by confocal microscopy (LSM510; Carl Zeiss).

Statistical analysis

Each experiment was conducted at least three times with consistent results. The gel or blot representative of each experiment is presented in this study. The statistical significance was analyzed using Student's *t*-test or Tukey's test.

Acknowledgements

We wish to thank K. Kuroiwa for technical assistance, our laboratory members for valuable discussions. This work was supported in part by research grants from the Ministry of Education, Culture, Sports, Science, and Technology of Japan.

References

Brunger, A.T. & DeLaBarre, B. (2003) NSF and p97/VCP: similar at first, difference at last. *FEBS Lett.* **555**, 126–133.

Custer, S.K., Neumann, M., Lu, H., Wright, A.C. & Taylor, J.P. (2010) Transgenic mice expressing mutant forms VCP/p97 recapitulate the full spectrum of IBMPFD including degeneration in muscle, brain and bone. *Hum. Mol. Genet.* **19**, 1741–1755.

Dalal, S. & Hanson, P.I. (2001) Membrane traffic: what drives the AAA motor? *Cell* **104**, 5–8.

Djamshidian, A., Schaefer, J., Haubenberger, D., Stogmann, E., Zimprich, F., Auff, E. & Zimprich, A. (2009) A novel mutation in the VCP gene (G157R) in a German family with inclusion-body myopathy with Paget disease of bone and frontotemporal dementia. *Muscle Nerve* **39**, 389–391.

Dreveny, I., Pye, V.E., Beuron, F., Briggs, L.C., Isaacson, R.L., Matthews, S.J., McKeown, C., Yuan, X., Zhang, X. & Freemont, P.S. (2004) p97 and close encounters of every kind: a brief review. *Biochem. Soc. Trans.* **32**, 715–720.

Forman, M.S., Mackenzie, I.R., Cairns, N.J., Swanson, E., Boyer, P.J., Drachman, D.A., Jhaveri, B.S., Karlawish, J.H., Pestronk, A., Smith, T.W., Tu, P.H., Watts, G.D., Markesbery, W.R., Smith, C.D. & Kimonis, V.E. (2006) Novel ubiquitin neuropathology in frontotemporal dementia with valosin-containing protein gene mutations. *J. Neuropathol. Exp. Neurol.* **65**, 571–581.

García-Mata, R., Bebök, Z., Sorscher, E.J. & Sztul, E.S. (1999) Characterization and dynamics of aggresome formation by a cytosolic GFP-chimera. *J. Cell Biol.* **146**, 1239–1254.

Haubenberger, D., Bittner, R.E., Rauch-Shorny, S., Zimprich, F., Mannhalter, C., Wagner, L., Mineva, I., Vass, K., Auff, E. & Zimprich, A. (2005) Inclusion body myopathy and Paget disease is linked to a novel mutation in the VCP gene. *Neurology* **65**, 1304–1305.

Higashiyama, H., Hirose, F., Yamaguchi, M., Inoue, Y.H., Fujikake, N., Matsukage, A. & Kakizuka, A. (2002) Identification of *ter94*, Drosophila *VCP*, as a modulator of polyglutamine-induced neurodegeneration. *Cell Death Differ.* **9**, 264–273.

Hirabayashi, M., Inoue, K., Tanaka, K., Nakadate, K., Ohsawa, Y., Kamei, Y., Popiel, A.H., Sinohara, A., Iwamatsu, A., Kimura, Y., Uchiyama, Y., Hori, S. & Kakizuka, A. (2001) VCP/p97 in abnormal protein aggregates, cytoplasmic vacuoles, and cell death, phenotypes relevant to neurodegeneration. *Cell Death Differ.* **8**, 977–984.

Hübbers, C.U., Clemen, C.S., Kesper, K., *et al.* (2007) Pathological consequences of VCP mutations on human striated muscle. *Brain* **130**, 381–393.

Ishigaki, S., Hishikawa, N., Niwa, J., Iemura, S., Natsume, T., Hori, S., Kakizuka, A., Tanaka, K. & Sobue, G. (2004) Physical and functional interaction between dorfin and valosin-containing protein that are colocalized in ubiquitylated inclusions in neurodegenerative disorders. *J. Biol. Chem.* **279**, 51376–51385.

Johnston, J.A., Illing, M.E. & Kopito, R.R. (2002) Cytoplasmic dynein/dynactin mediates the assembly of aggresomes. *Cell Motil. Cytoskeleton* **53**, 26–38.

Johnston, J.A., Ward, C.L. & Kopito, R.R. (1998) Aggresomes: a cellular response to misfolded proteins. *J. Cell Biol.* **143**, 1883–1898.

Ju, J.S., Fuentealba, R.A., Miller, S.E., Jackson, E., Piwnica-Worms, D., Baloh, R.H. & Weihl, C.C. (2009) Valosin-containing protein (VCP) is required for autophagy and is disrupted in VCP disease. *J. Cell Biol.* **87**, 875–888.

Ju, J.S., Miller, S.E., Hanson, P.I. & Weihl, C.C. (2008) Impaired protein aggregate handling and clearance underlie the pathogenesis of p97/VCP-associated disease. *J. Biol. Chem.* **283**, 30289–30299.

Kawaguchi, Y., Kovacs, J.J., McLaurin, A., Vance, J.M., Ito, A. & Yao, T.P. (2003) The deacetylase HDAC6 regulates aggresome formation and cell viability in response to misfolded protein stress. *Cell* **115**, 727–738.

Kawaguchi, Y., Okamoto, T., Taniwaki, M., Aizawa, M., Inoue, M., Katayama, S., Kawakami, H., Nakamura, S., Nishimura, M., Akiguchi, I., Kimura, J., Narumiya, S. & Kakizuka, A. (1994) CAG expansions in a novel gene for Machado-Joseph disease at chromosome 14q32.1. *Nat. Genet.* **8**, 221–228.

Kimonis, V.E., Kovach, M.J., Waggoner, B., Leal, S., Salam, A., Rimer, L., Davis, K., Khardori, R. & Gelber, D. (2000) Clinical and molecular studies in a unique family with autosomal dominant limb-girdle muscular dystrophy and Paget disease of bone. *Genet. Med.* **2**, 232–241.

Kimonis, V.E., Mehta, S.G., Fulchiero, E.C., Thomasova, D., Pasquali, M., Boycott, K., Neilan, E.G., Kartashov, A., Forman, M.S., Tucker, S., Kimonis, K., Mumm, S., Whyte, M.P., Smith, C.D. & Watts, G.D. (2008) Clinical studies in familial VCP myopathy associated with Paget disease of

bone and frontotemporal dementia. *Am. J. Med. Genet. A.* **146A**, 745–757.

Kimonis, V.E. & Watts, G.D. (2005) Autosomal dominant inclusion body myopathy, Paget disease of bone, and frontotemporal dementia. *Alzheimer Dis. Assoc. Disord.* **19**, S44–S47.

Kobayashi, T., Manno, A. & Kakizuka, A. (2007) Involvement of valosin-containing protein (VCP)/p97 in the formation and clearance of abnormal protein aggregates. *Genes Cells* **12**, 889–901.

Kobayashi, T., Tanaka, K., Inoue, K. & Kakizuka, A. (2002) Functional ATPase activity of p97/VCP is required for the quality control of endoplasmic reticulum in neuronally differentiated mammalian PC12 cells. *J. Biol. Chem.* **277**, 47358–47365.

Koike, M., Fukushi, J., Ichinohe, Y., Higashimae, N., Fujishiro, M., Sasaki, C., Yamaguchi, M., Uchihara, T., Yagishita, S., Ohizumi, H., Hori, S. & Kakizuka, A. (2010) Valosin-containing protein (VCP) in novel feedback machinery between abnormal protein accumulation and transcriptional suppression. *J. Biol. Chem.* in press.

Kovach, M.J., Waggoner, B., Leal, S.M., *et al.* (2001) Clinical delineation and localization to chromosome 9p13.3-p12 of a unique dominant disorder in four families: hereditary inclusion body myopathy, Paget disease of bone, and frontotemporal dementia. *Mol. Genet. Metab.* **74**, 458–475.

Mizuno, Y., Hori, S., Kakizuka, A. & Okamoto, K. (2003) Vacuole-creating protein in neurodegenerative diseases in humans. *Neurosci. Lett.* **343**, 77–80.

Mori-Konya, C., Kato, N., Maeda, R., Yasuda, K., Higashimae, N., Noguchi, M., Koike, M., Kimura, Y., Ohizumi, H., Hori, S. & Kakizuka, A. (2009) p97/valosin-containing protein (VCP) is highly modulated by phosphorylation and acetylation. *Genes Cells* **14**, 483–497.

Noguchi, M., Takata, T., Kimura, Y., Manno, A., Murakami, K., Koike, M., Ohizumi, H., Hori, S. & Kakizuka, A. (2005) ATPase activity of p97/valosin-containing protein is regulated by oxidative modification of the evolutionally conserved cysteine 522 residue in Walker A motif. *J. Biol. Chem.* **280**, 41332–41341.

Nowis, D., McConnell, E. & Wójcik, C. (2006) Destabilization of the VCP-Ufd1-Npl4 complex is associated with decreased levels of ERAD substrates. *Exp. Cell Res.* **312**, 2921–2932.

Schröder, R., Watts, G.D., Mehta, S.G., Evert, B.O., Broich, P., Fliessbach, K., Pauls, K., Hans, V.H., Kimonis, V. & Thal, D.R. (2005) Mutant valosin-containing protein causes a novel type of frontotemporal dementia. *Ann. Neurol.* **57**, 457–461.

Wang, Q., Song, C. & Li, C.C. (2004) Molecular perspectives on p97-VCP: progress in understanding its structure and diverse biological functions. *J. Struct. Biol.* **146**, 44–57.

Watts, G.D., Thomasova, D., Ramdeen, S.K., Fulchiero, E.C., Mehta, S.G., Drachman, D.A., Weihl, C.C., Jamrozik, Z., Kwiecinski, H., Kaminska, A. & Kimonis, V.E. (2007) Novel VCP mutations in inclusion body myopathy associated with Paget disease of bone and frontotemporal dementia. *Clin. Genet.* **72**, 420–426.

Watts, G.D., Wymer, J., Kovach, M.J., Mehta, S.G., Mumm, S., Darvish, D., Pestronk, A., Whyte, M.P. & Kimonis, V.E. (2004) Inclusion body myopathy associated with Paget disease of bone and frontotemporal dementia is caused by mutant valosin-containing protein. *Nat. Genet.* **36**, 377–381.

Weihl, C.C., Dalal, S., Pestronk, A. & Hanson, P.I. (2006) Inclusion body myopathy-associated mutations in p97/VCP impair endoplasmic reticulum-associated degradation. *Hum. Mol. Genet.* **15**, 189–199.

Weihl, C.C., Pestronk, A. & Kimonis, V.E. (2009) Valosin-containing protein disease: inclusion body myopathy with Paget's disease of the bone and fronto-temporal dementia. *Neuromuscul. Disord.* **19**, 308–315.

Zhang, X., Shaw, A., Bates, P.A., Newman, R.H., Gowen, B., Orlova, E., Gorman, M.A., Kondo, H., Dokurno, P., Lally, J., Leonard, G., Meyer, H., van Heel, M. & Freemont, P.S. (2000) Structure of the AAA ATPase p97. *Mol. Cell* **6**, 1473–1484.

Received: 8 February 2010
Accepted: 12 May 2010

Supporting Information/Supplementary material

The following Supporting Information can be found in the online version of the article:

Table S1 List of siRNA sequences used in this work

Video S1 Time-lapse analysis of aggresome formation in cells expressing GFP-tagged VCP.

Additional Supporting Information may be found in the online version of this article.

Please note: Wiley-Blackwell are not responsible for the content or functionality of any supporting materials supplied by the authors. Any queries (other than missing material) should be directed to the corresponding author for the article.

nature neuroscience

Ontogeny-recapitulating generation and tissue integration of ES cell–derived Purkinje cells

Keiko Muguruma[1], Ayaka Nishiyama[1], Yuichi Ono[2], Hiroyuki Miyawaki[3], Eri Mizuhara[2], Seiji Hori[4], Akira Kakizuka[4], Kunihiko Obata[5], Yuchio Yanagawa[6,7], Tomoo Hirano[3] & Yoshiki Sasai[1]

Purkinje cells are the sole output neurons of the cerebellar cortex and their dysfunction causes severe ataxia. We found that Purkinje cells could be robustly generated from mouse embryonic stem (ES) cells by recapitulating the self-inductive signaling microenvironments of the isthmic organizer. The cell-surface marker Neph3 enabled us to carry out timed prospective selection of Purkinje cell progenitors, which generated morphologically characteristic neurons with highly arborized dendrites that expressed mature Purkinje cell–specific markers such as the glutamate receptor subunit GluRδ2. Similar to mature Purkinje cells, these neurons also showed characteristic spontaneous and repeated action potentials and their postsynaptic excitatory potentials were generated exclusively through nonNMDA glutamate receptors. Fetal transplantation of precursors isolated by fluorescence-activated cell sorting showed orthotopic integration of the grafted neurons into the Purkinje cell layer with their axons extending to the deep cerebellar nuclei and dendrites receiving climbing and parallel fibers. This selective preparation of bona fide Purkinje cells should aid future investigation of this important neuron.

During embryonic development, the cerebellar anlage arises from two distinct tissues in dorsal rhombomere 1 adjacent to the fourth ventricle[1–3]: the cerebellar ventricular zone, which expresses the basic helix-loop-helix (bHLH) transcription factor Ptf1a, and the rhombomere 1 rhombic lip, which expresses another bHLH factor, Math1. The Ptf1a$^+$ progenitors produce GABAergic neurons of the cerebellar cortex (Purkinje, basket, stellate and Golgi neurons) and of the deep cerebellar nuclei (DCN)[4]. In contrast, Math1$^+$ progenitors generate cerebellar glutamatergic neurons, including granule cells and large DCN projection neurons[5–7].

The initial phase of cerebellar development depends on the formation and function of the isthmic organizer[8], which lies at the midbrain-hindbrain boundary (MHB). This organizer is formed by the intricate regulatory functions of region-specific transcription factors such as En1/2, Pax2/5/8, Otx2 and Gbx2 (refs. 8–11). The expression of these factors is under the control of fibroblast growth factor 8 (Fgf8) secreted by the isthmic organizer itself[9–11]. Mutant mice with reduced *Fgf8* expression have a severe defect in cerebellar development[12], whereas Fgf8 misexpression in the chick brain forms ectopic cerebellar tissues[13]. Following the onset of Fgf8 expression, the expression of another key signaling factor, Wnt1, starts in the MHB. These two factors form a positive autofeedback loop to drive each other's expression that also involves the expression of transcription factors such as En2 and Pax2 (refs. 14–16). In addition, Fgf8 and Wnt1 act as organizer factors that pattern the tissues around the MHB. This self-inducing feature of isthmic organizer development presumably contributes to its potent patterning ability and to the robust maintenance of its tissue identity after ectopic transplantation to other brain regions.

Among the cerebellar neurons, Purkinje cells have a central role in integrating heterogeneous neural inputs from the mossy and climbing fibers. Purkinje cell dysfunction (hereditary or acquired) leads to severe motor discoordination. Math1$^+$ granule cell progenitors are generated from ES cells at a relatively high efficiency (>15%) in serum-free suspension culture (serum-free culture of embryoid body–like aggregates or SFEB[17]) in the presence of bone morphogenetic protein (BMP) and Wnt signals[18]. In contrast, although ES cells can be induced to differentiate into Purkinje cells when treated with Fgf8 and Wnt ligands, their production is quite inefficient, with Purkinje cells typically comprising less than 1% of the total[18–20].

Therefore, we took a different strategy that focuses on the initiation of the endogenous program for self-inducing isthmic development and successfully applied it to the efficient differentiation of ES cells into functional Purkinje cells, using a modified SFEB culture (SFEBq)[21,22].

RESULTS

Transient Fgf treatment induces isthmus/rhombomere 1 tissues

Although *En2* is initially expressed in a broad domain of the mes- and metencephalon, during early cerebellar development (embryonic day (E)12.5), En2 (clearly detectable by immunofluorescence) is strongly expressed mainly in the MHB and its neighboring regions[8,23] (the isthmic/rhombomere 1 (Otx2$^-$) region and the caudal-most midbrain region, just rostral to the isthmus (Otx2$^+$; **Fig. 1a**)). Hereafter, these En2$^+$ tissues are referred as MHB-proximity tissues.

[1]Organogenesis and Neurogenesis Group, RIKEN Center for Developmental Biology, Kobe, Japan. [2]Group for Neuronal Differentiation, KAN Institute, Kobe, Japan. [3]Department of Biophysics, Graduate School of Science, Kyoto University, Kyoto, Japan. [4]Laboratory of Functional Biology, Graduate School of Biostudies, Kyoto University, Kyoto, Japan. [5]Obata Research Unit, RIKEN Brain Science Institute, Wako, Japan. [6]Department of Genetic and Behavioral Neuroscience, Gunma University Graduate School of Medicine, Maebashi, Japan. [7]Japan Science and Technology Agency, CREST, Tokyo, Japan. Correspondence should be addressed to Y.S. (yoshikisasai@cdb.riken.jp).

Received 12 July; accepted 13 August; published online 12 September 2010; doi:10.1038/nn.2638

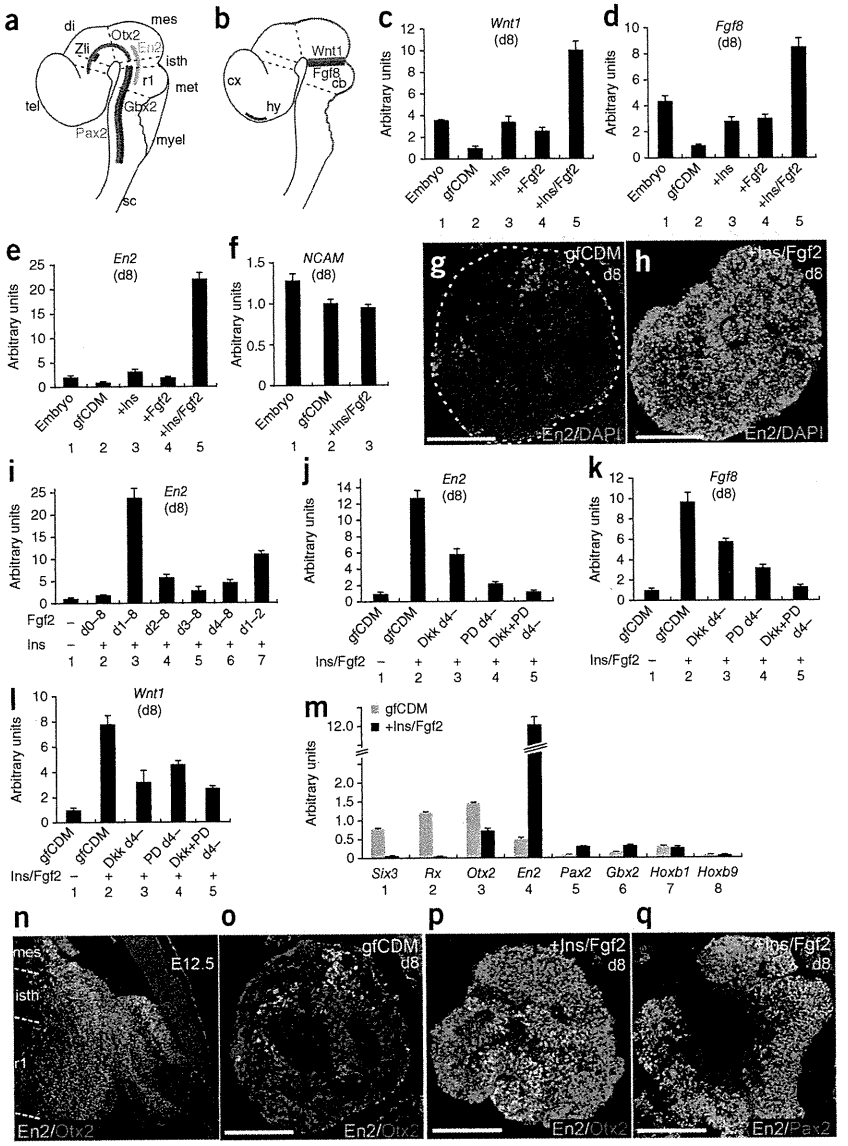

Figure 1 Fgf2 and insulin cooperatively induce generation of midbrain-hindbrain identity in ES cells in SFEBq culture. (**a**,**b**) Expression of markers in the embryonic neural tube (E12.5 mouse). (**a**) Otx2 (red), En2 (green), Gbx2 (blue) and Pax2 (purple). (**b**) *Wnt1* (red) and *Fgf8* (blue). As well as the MHB region, Wnt1 is expressed in the dorsal-most domain of the neural tube and Fgf8 is expressed in the rostral forebrain. (**c**–**f**) qPCR analysis of SFEBq-cultured ES cell aggregates on day 8 for the expression of *Wnt1* (**c**), *Fgf8* (**d**), *En2* (**e**) and *NCAM* (**f**) (n = 120 aggregates from 5 independent experiments). Total RNA from E11.5 whole embryos (lane 1) was used as a control. (**g**,**h**) Cryosections of SFEBq-cultured ES cell aggregates on day 8. ES cells were cultured in gfCDM alone (**g**) or containing insulin and Fgf2 (**h**). Sections were immunostained with anti-En2 antibody and counterstained with DAPI. Broken white line shows outline of an aggregate. (**i**–**m**) qPCR analysis of SFEBq-cultured ES cell aggregates on day 8 for the expression of *En2* (**i**,**j**), *Fgf8* (**k**), *Wnt1* (**l**) and regional markers along the rostral-caudal axis (**m**) (n = 140 aggregates from 5 independent experiments). Dkk (250 ng ml^{-1}) and/or PD173074 (10 nM) were added to culture on day 4. (**n**) Sagittal section of mouse mesencephalon/metencephalon at E12.5, immunostained with antibodies to En2 and Otx2. (**o**–**q**) Cryosections of SFEBq-cultured ES cell aggregates on day 8. ES cells were cultured in gfCDM alone (**o**) or containing insulin and Fgf2 (**p**,**q**). Sections were immunostained with antibodies to En2 (**o**–**q**), Otx2 (**o**,**p**) and Pax2 (**q**). tel, telencephalon; di, diencephalon; mes, mescencephalon; met, metencephalon; myel, myelencephalon; sc, spinal cord; isth, isthmus; rhombomere 1, rhombomere 1; cx, cortex; hy, hypothalamus; cb, cerebellum. Scale bars, 100 μm. Error bars represent s.e.m.

When totally growth factor–free, chemically defined medium (gfCDM)[21] is used, ES cell aggregates cultured in the SFEBq method selectively differentiate into rostral forebrain tissues that express the forebrain-specific transcription factors Six3 and Rx[21], but not into En2$^+$ tissues. We first investigated the effects of Fgf8 and Wnt signals, which are expressed in the MHB-proximity region (**Fig. 1b**), on the induction of En2. However, the percentage of En2$^+$ cells did not exceed 15% of total cells on day 8 under any of the conditions tested (up to 200 ng ml^{-1}), suggesting that MHB development can be only partly recapitulated *in vitro* by exogenous Fgf8 and Wnt. With this in mind, we employed a different strategy that makes use of endogenous Fgf8 and Wnt1 as local organizing factors.

Previous results suggest that the addition of insulin (on days 0–8) has a moderate caudalizing activity, particularly when added to gfCDM culture[21]. Indeed, insulin treatment suppressed the expression of *Six3* and *Rx* (**Supplementary Fig. 1**), and moderately increased the expression of *Wnt1*, *Fgf8* and *En2* (<3-fold on day 8; **Fig. 1c–e**). There is evidence that Fgf2 has rhombomere 1–inducing activity in an embryonic neural explant assay[24]. Consistent with this, when Fgf2 (20 ng ml^{-1}) was added to the culture from day 1 along with insulin, the expression of *Wnt1* and *Fgf8* was substantially induced on both day 8 (eight- and ten-fold, respectively; **Fig. 1c**,**d**) and day 5 (**Supplementary Fig. 1**). The synergistic effect of Fgf2 and insulin on *En2* expression was particularly high (20-fold on day 8; **Fig. 1e**) whereas general neural differentiation was unaffected (**Fig. 1f**). The majority (>80%) of cells in the SFEBq aggregates were strongly immunoreactive for En2 on day 8 (**Fig. 1g**,**h**). Thus, treatment with Fgf2 and insulin promoted *Wnt1* and *Fgf8* expression and induced nearly selective differentiation into En2$^+$ tissues. Fgf2 was at least twice as effective at inducing the expression of *En2* and *Fgf8* than Fgf4, 5 or 8 when added to culture on day 1 (**Supplementary Fig. 1**).

We did not observe clear En2 induction when the Fgf2 treatment was started on day 0 (instead of day 1), showing that its addition on day 0 has an inhibitory effect (**Fig. 1i**). In contrast, even transient Fgf2 treatment from day 1 to day 2 was sufficient to substantially induce En2$^+$ tissues (**Fig. 1i**). Fgf2 treatment on days 2–8 was substantially less effective than on days 1–8 (**Fig. 1i**). Given that neural differentiation starts around day 3 in SFEBq culture[21] (the cells instead express epiblast markers during days 1–3; data not shown), the main role of Fgf2 was probably to confer selective competence on differentiating ES cell aggregates before neural differentiation,

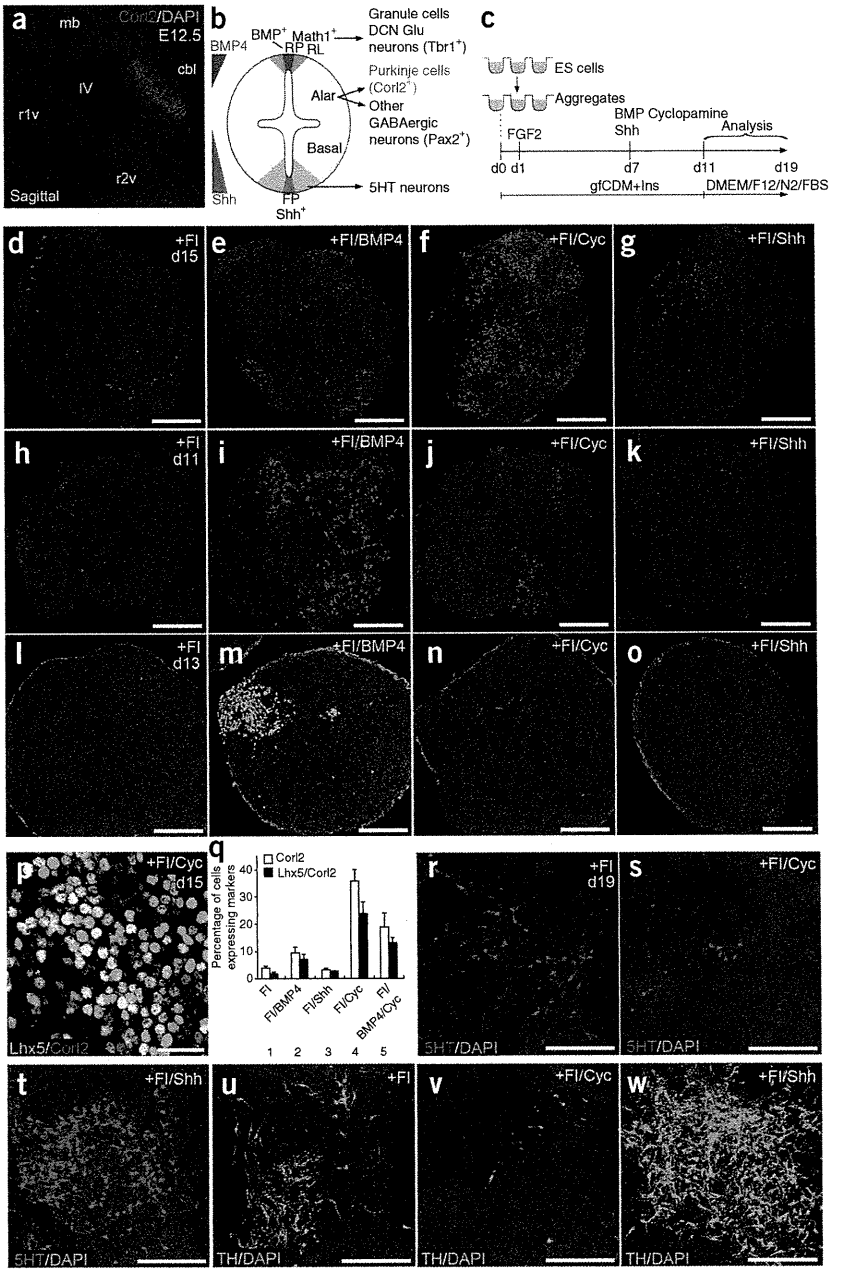

Figure 2 Sequential treatment of Fgf2 and a Shh inhibitor in the presence of insulin induces cerebellar plate precursors in SFEBq culture. (**a**) Expression of Corl2 (red) in a sagittal section of mouse hindbrain. Cells of the cerebellar plate express Corl2. (**b**) Schematic diagram showing dorsal-ventral patterning of the rostral hindbrain. (**c**) Procedure for ES cell culture. BMP4 (1 nM), Shh (30 nM) or cyclopamine (10 μM) was added on day 7. (**d–o**) Sections of ES cell aggregates treated with Fgf2 (**d**,**h**,**l**), Fgf2 and BMP4 (**e**,**i**,**m**), Fgf2 and cyclopamine (**f**,**j**,**n**), or Fgf2 and Shh (**g**,**k**,**o**). The cells were immunostained with antibodies to Corl2 on day 15 (**d–g**), Math1 on day 11 (**h–k**) or Tbr1 on day 13 (**l–o**). Nuclei were counterstained with DAPI. (**p**) Expression of Lhx5 and Corl2 in ES cell aggregate treated with Fgf2 and cyclopamine. (**q**) Percentage of cells positive for Corl2 (open) and double-positive for Lhx5 and Corl2 (closed) in ES cell aggregates ($n = 24$ aggregates from three independent experiments). (**r–w**) Differentiation of 5HT-positive (**r–t**) and tyrosine hydroxylase–positive (**u–w**) neurons by treatment with Fgf2 (**r**,**u**), Fgf2 and cyclopamine (**s**,**v**) and Fgf2 and Shh (**t**,**w**). RP, roof plate; FP, floor plate; mb, midbrain; cbl, cerebellar plate; r1v, ventral region of rhombomere 1; r2v, ventral region of rhombomere 2; IV, fourth ventricle. Scale bars: 100 μm (**d–o**); 200 μm (**p–u**); 25 μm (**w**). Error bars represent s.e.m.

and to bias the cells' differentiation toward midbrain-hindbrain regionality. In addition, the increased expression of *En2*, *Fgf8* and *Wnt1* was inhibited by the late addition of the Fgf inhibitor PD173074 or the Wnt inhibitor Dkk1 (day 4 onwards; **Fig. 1j–l**). This result supports the idea that the endogenous isthmic organizer factors Fgf8 and Wnt1 (or related proteins) were induced as a secondary effect of the transient Fgf2 treatment (in the presence of insulin), and that their activities are essential for the induction of En2 and the maintenance of their own expression *in vitro*, as *in vivo*.

The coordinated control of regional marker expression in SFEBq culture with Fgf2 and insulin (FI) treatment (SFEBq/FI) was also confirmed by qPCR analysis. Forebrain markers (*Six3*, *Rx* and *Otx2*) were suppressed, and MHB-proximity markers (*En2*, *Pax2* and *Gbx2*) were increased, but there was little effect on more caudal markers (*Hoxb1* and *b9*; **Fig. 1m**).

In the embryonic brain (E12), Otx2 is expressed in both the forebrain and midbrain, but not in the hindbrain or isthmus (**Fig. 1n**). At this stage, En2 is coexpressed with Otx2 exclusively in the caudal-most midbrain (yellow in **Fig. 1n**), but not in the isthmus/rhombomere 1 region (green). SFEBq/gfCDM–cultured aggregates, which rarely contained En2$^+$ cells, mostly consisted of Otx2$^+$/En2$^-$ cells (**Fig. 1o**), consistent with their forebrain-dominant nature[21]. In contrast, SFEBq/FI–cultured aggregates contained few Otx2$^+$/En2$^-$ cells (<5%). The majority of the cells (>70%) were Otx2$^-$/En2$^+$ (isthmus/rhombomere 1 type), and 10–20% of the En2$^+$ cells coexpressed Otx2 (caudal midbrain type) (**Fig. 1p** and **Supplementary Fig. 1**). These findings suggested that a substantial population of the En2$^+$ cells that were induced in SFEBq/FI culture had regional characteristics of the isthmus/rhombomere 1. Concordantly, ~60% of the En2$^+$ cells coexpressed Pax2 (**Fig. 1q** and **Supplementary Fig. 1**), which colocalizes with En2 *in vivo* only in the embryonic isthmic/rhombomere 1 region but not in the midbrain area (**Supplementary Fig. 1**). These findings indicate that the SFEBq/FI culture supports the efficient and selective differentiation of ES cell–derived neural progenitors into En2$^+$ tissues, particularly with isthmus/rhombomere 1 characteristics (**Supplementary Fig. 1**).

Cerebellar precursors specified by passive dorsalization

The transcriptional corepressor Corl2 (**Fig. 2a**,**b**) is a very early Purkinje cell marker (E12 onwards) that is not expressed in other

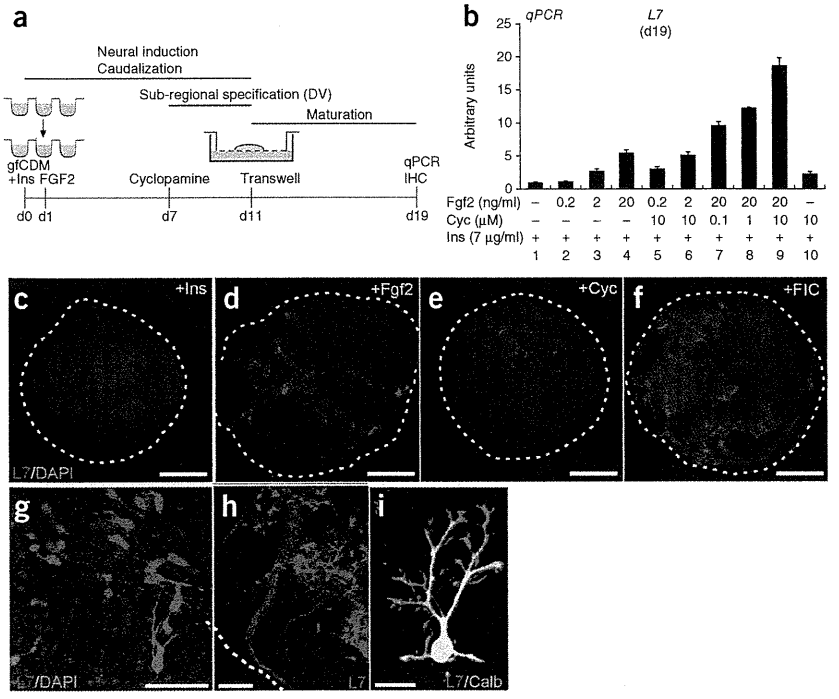

Figure 3 Generation of Purkinje cells in SFEBq/FIC culture in Transwell culture. (**a**) Procedure for the differentiation of Purkinje cells from ES cell culture. Treated aggregates were cultured on a Transwell membrane and analyzed on day 19. (**b**) qPCR analysis of *L7* expression by ES cell aggregates treated with different concentrations of Fgf2 and cyclopamine ($n = 140$ aggregates from 5 independent experiments). (**c–f**) Aggregates were treated with insulin (**c**), Fgf2 (**d**), cyclopamine (**e**) or all three (FIC; **f**) and immunostained for L7. Aggregates are outlined by a broken white line. (**g–j**) High-magnification view of aggregates treated with insulin + Fgf2 + cyclopamine. (**h**) Fasciculated L7-positive axons run in the aggregate. White broken line demarcates the outline of the aggregate. (**i**) A cell co-expressing L7 and calbindin extends dendrites, showing a typical Purkinje cell morphology. Scale bars: 150 μm (**c–f**); 50 μm (**g**); 100 μm (**h**); 20 μm (**i**). Error bars represent s.e.m.

cerebellar neurons[25]. Using Corl2 as an indicator, we searched for conditions to optimize Purkinje cell precursor generation by modifying dorsal-ventral specification (**Fig. 2c–o**).

During early cerebellar development (E10–11 for mouse), Purkinje cell precursors arise exclusively from the cerebellar neuroepithelium on the alar plate of rhombomere 1, which subsequently contributes to the genesis of the cerebellar plate[3] (light blue in **Fig. 2b**). The dorsal tip of the rhombomere 1 alar plate forms the rhombic lip (**Fig. 2b**), which generates the Math1$^+$ granule cells of the cerebellar cortex and the DCN glutamatergic neurons positive for the transcriptional factor Tbr1 (ref. 7). The basal plate of rhombomere 1 develops into the main body of the pons, and its ventral-most region generates serotonergic (5HT$^+$) neurons. Midbrain dopaminergic neurons expressing tyrosine hydroxylase arise just rostrally to this region.

BMP signals, which emanate from the roof plate (**Fig. 2b**), have an inductive function in the dorsal specification of rhombomere 1 tissues[26]. In contrast, sonic hedgehog (Shh) derived from the floor plate promotes neural ventralization[24,27]. Treatment with BMP4 on days 7–11 induced the expression of the dorsal-most neuronal markers Math1 and Tbr1 (**Figs. 2i,m**; Tbr1$^+$ neurons always clustered). These cells also expressed Pax6, which is a marker for granule cells, and Meis1 and 2, which are DCN markers (**Supplementary Fig. 2**). However, BMP4 did not substantially increase the number of Corl2$^+$ cells (**Fig. 2e**).

We therefore took an alternative approach, to promote dorsalization indirectly. Cyclopamine antagonizes hedgehog receptors, thereby shutting off the ventralizing effect of endogenous Shh in ES cell aggregates. As we hoped, cyclopamine treatment (days 7–11) caused a marked increase in the Corl2$^+$ population (35.7 ± 4.5% of total cells) in SFEBq/FI culture (**Fig. 2f**), but not in the Math1$^+$ or Tbr1$^+$ populations (**Fig. 2j,n**). Three-quarters of Corl2$^+$ precursors coexpressed Lhx5, another marker for Purkinje cell precursors (**Fig. 2p,q**). Combined treatment with BMP4 and cyclopamine did not increase the percentage of Corl2$^+$ cells (18.9 ± 5.1%; **Fig. 2q**) or Math1$^+$ cells (**Supplementary Fig. 2**).

As expected, Shh was clearly detectable in the SFEBq/FI aggregates by qPCR on day 8 (data not shown). In addition, the differentiation of 5HT$^+$ and tyrosine hydroxylase-positive neurons (which are Shh-dependent *in vivo*) in the aggregate was completely inhibited by cyclopamine, whereas exogenous Shh treatment markedly increased the number of 5HT$^+$ and tyrosine hydroxylase-positive neurons (**Fig. 2r–w**), without promoting the expression of Corl2, Math1 or Tbr1 (**Fig. 2g,k,o**). The anti-ventralizing (passive dorsalization) effect of cyclopamine was confirmed by the qPCR analysis of dorsoventral marker expression (**Supplementary Fig. 2**). Cyclopamine treatment suppressed the basal plate markers *Nkx2.2*, *Nkx6.1* and *Olig2* and elevated the expression of the dorsal markers *Pax7* and *Corl2*, whereas the intermediate dorsoventral marker *Dbx2* and the dorsal-most marker *Zic1* were mostly unaffected. These findings indicate that Corl2$^+$ Purkinje cell–like precursors are efficiently produced in SFEBq/FI culture with the additional anti-ventralizing effect of cyclopamine (SFEBq/FIC, hereafter).

Efficient differentiation of Purkinje cells

We cultured SFEBq/FIC aggregates en bloc on a porous membrane (Transwell culture[21,22] during days 11–19; **Fig. 3a**) to neuronal maturation in long-term culture. The combination of cyclopamine and Fgf2 (**Fig. 3b–f**) efficiently induced the differentiation of Purkinje cells expressing the lineage-specific marker L7 in the ES cell–derived neural tissues (42.6 ± 5.2% of total neurons; **Fig. 3f**). A qPCR analysis showed that *L7* induction was about 20-fold more efficient under these conditions than with insulin treatment alone (**Fig. 3b**). Within these neural tissues, most L7$^+$ cells were found in clusters (**Fig. 3f,g**), and their axons frequently formed long fascicles that extended circumferentially at the periphery of the tissues (**Fig. 3h**). On day 19, L7$^+$ cells were positive for calbindin and Corl2 (**Fig. 3i** and data not shown).

Exposure to cyclopamine on days 7–8 was sufficient to promote L7$^+$ cell differentiation (**Supplementary Fig. 3**) and to shut off endogenous *Shh* expression (not shown). In contrast, Fgf2 treatment was most effective for *L7* induction from days 1–11. It was ~50% and 10% as efficient, respectively, when added from days 1–4 or days 4–11 (**Supplementary Fig. 3**). Fgf4 and Fgf8 (days 1–11) also qualitatively promoted *L7* expression in the presence of insulin and cyclopamine, but not as efficiently as Fgf2 at 20 ng ml^{-1} (**Supplementary Fig. 3**)

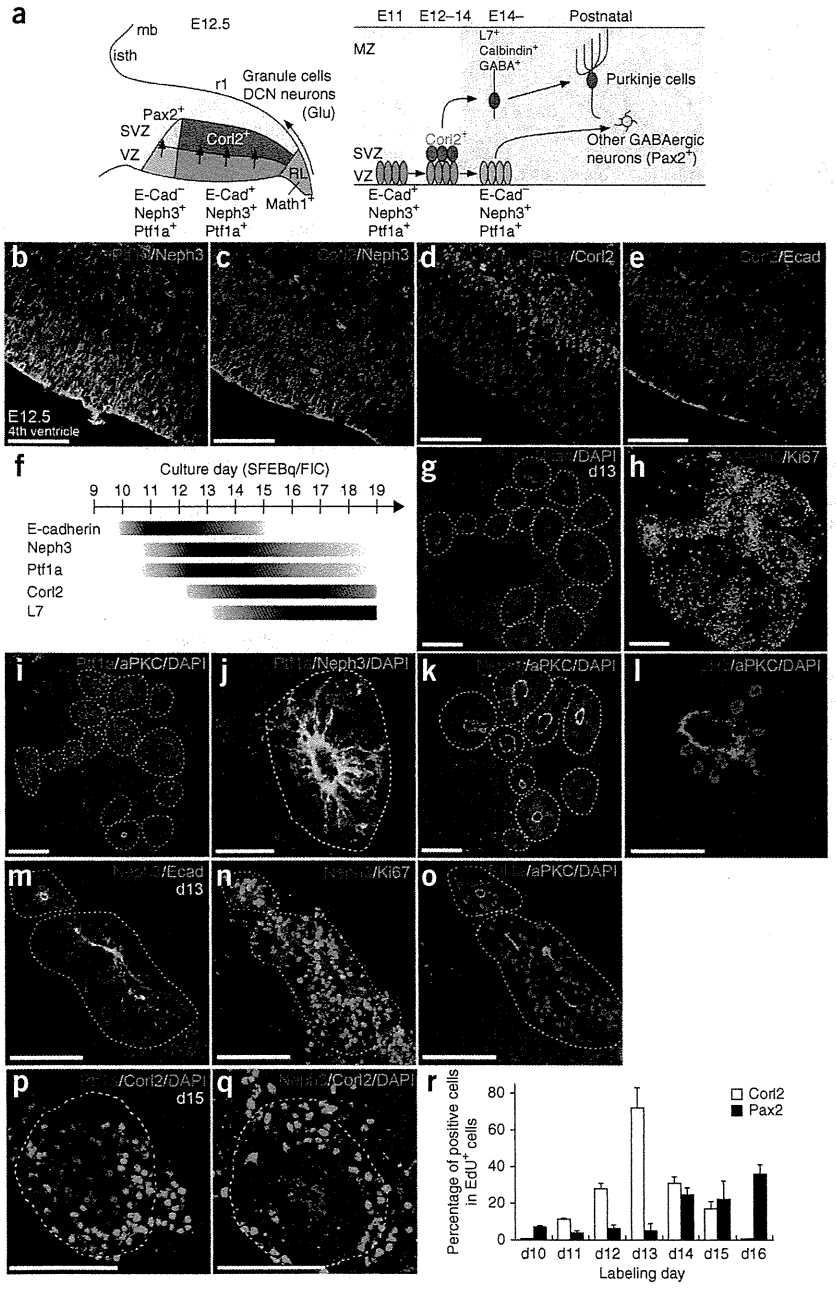

Figure 4 ES cell–derived neuroepithelial rosettes express cerebellar progenitor markers in SFEBq culture. (**a**) Schematic diagram showing the organization of the cerebellar plate (left, sagittal view) and the ontogenesis of cerebellar neurons (right). (**b–e**) Expression of cerebellar progenitor markers in the E12.5 mouse cerebellar plate. Neph3 (**b**,**c**), E-cadherin (**e**) and Ptf1a (**b**,**d**) were expressed in the mitotic neuroepithelium, whereas Corl2 (**c–e**) was expressed in postmitotic cells. (**f**) Temporal expression of the markers in ES cell aggregates in SFEBq/FIC culture. (**g–i**) Adjacent sections of an aggregate on day 13, immunostained for N-cadherin (**g**), Neph3 and Ki67 (**h**) or Ptf1a and aPKC (**i**). Neural rosettes are demarcated by broken white lines. (**j**) High-magnification view of a Ptf1a$^+$ Neph3$^+$ neural rosette on day 13. (**k**) An aggregate on day 13, immunostained for Neph3 and aPKC. Neph3 was preferentially enriched at the aPKC$^+$ apical surface. (**l**) High-magnification view of a neural rosette on day 13, immunostained with pH3 and aPKC. (**m–o**) High-magnification view of adjacent sections of an aggregate on day 13, immunostained with Neph3 and E-cadherin (**m**), Neph3 and Ki67 (**n**) or Ptf1a and aPKC (**o**). (**p**,**q**) Adjacent sections of an aggregate on day 15, immunostained with Ptf1a and Corl2 (**p**) or Neph3 and Corl2 (**q**). (**r**) Percentage of EdU-positive cells expressing Corl2 (open columns) and Pax2 (closed columns) in aggregates on the indicated days (n = 56 aggregates from 3 independent experiments). Scale bars: 100 μm (**b–e**,**g–i**,**k**,**m–q**); 50 μm (**l**,**j**). Error bars represent s.e.m.

or 100 ng ml^{-1} (data not shown). The addition of Wnt decreased the induction of *L7* in SFEBq/FIC culture (**Supplementary Fig. 3**). Collectively, the timed treatment with insulin (day 0 onwards), Fgf2 (day 1 onwards) and cyclopamine (day 7 onwards) in SFEBq culture steered ES cells to sequentially acquire a neural fate, rhombomere 1/MHB regional identity and cerebellar plate characteristics, which together led to efficient Purkinje cell differentiation *in vitro*.

Recapitulation of early cerebellar plate development

In the early cerebellar primordium, the neuroepithelium begins to express tissue-specific marker genes on E11–E12. One such marker is Ptf1a, a transcription factor that is essential for the genesis of Purkinje cells and cerebellar GABAergic interneurons (**Fig. 4a**,**b**). The membrane molecule Neph3 is the product of a Ptf1a target gene[28]. *Ptf1a* and *Neph3* are expressed together in most of the cerebellar plate neuroepithelium (**Fig. 4b**), but not at the Math1$^+$ rhombic lip (**Fig. 4a**, left). The mouse cerebellar plate neuroepithelium gives rise to Purkinje cells and cerebellar GABAergic interneurons at distinct developmental stages: E11–E13 for Purkinje cells and E13–P15 for GABAergic interneurons[29,30]. Postmitotic Purkinje cell precursors become positive for the lineage-specific marker Corl2 while still in the subventricular zone (SVZ; **Figs. 4a** and **3c**,**d**). The cerebellar plate neuroepithelium coexpresses Corl2 and E-cadherin (with N-cadherin) with a spatiotemporal pattern that overlaps with Purkinje cell generation (E12–14)[28] (**Fig. 4e**).

The temporal expression pattern of Purkinje cell differentiation markers in SFEBq/FIC culture resembled the *in vivo* expression pattern (**Fig. 4f**). For instance, obvious *Neph3*$^+$ expression was induced on day 11 in a cyclopamine-dependent manner (**Supplementary Fig. 2**). On day 13 of SFEBq/FIC culture, a large number of N-cadherin$^+$ neural cells were still mitotic (Ki67$^+$) in culture (**Fig. 4g**,**h**), and a large portion of these cells formed characteristic epithelial-sphere structures (neural rosettes). Of these neural rosettes, 73.0 ± 6.6% were double-positive for Neph3 and Ptf1a (**Fig. 4h–j** and **Supplementary Fig. 4**). Each neural rosette had a fixed epithelial apico-basal polarity, with the apical side to the interior of the rosette and demarcated by strong N-cadherin and aPKC expression (**Fig. 4g**,**k**). High mitotic

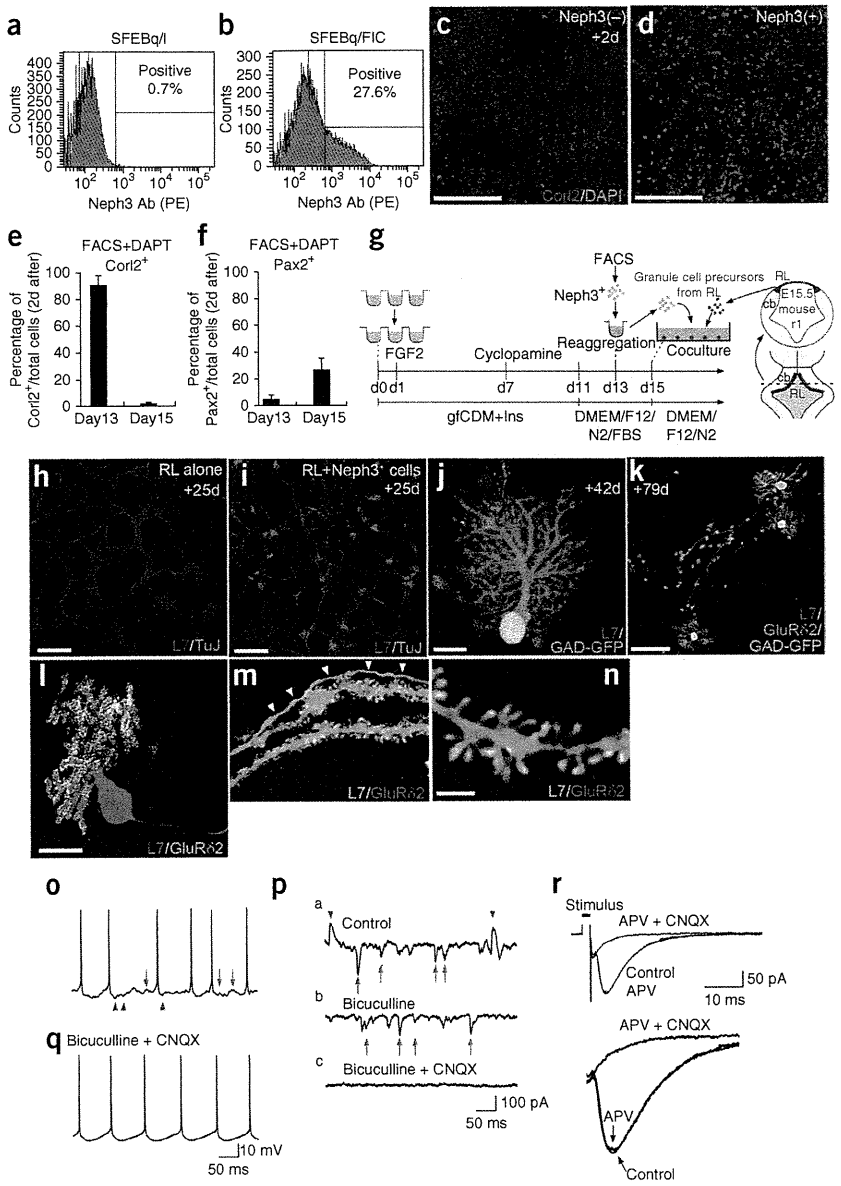

Figure 5 Nephn3+ progenitors on day 13 in SFEBq/FIC culture efficiently generate Purkinje cells with morphological and functional characteristics. (**a**,**b**) FACS analysis of ES cell aggregates on day 13 of SFEBq culture in the presence of insulin alone (**a**) or insulin, Fgf2 and cyclopamine (**b**). (**c**,**d**) Adhesion culture of Nephn3-positive (**c**) and Nephn3-negative (**d**) cells after FACS sorting, immunostained with Corl2. (**e**,**f**) Percentage of the cells expressing Corl2 (**e**) and Pax2 (**f**) in aggregates 2 days after FACS sorting and DAPT treatment on day 13 or 15 of SFEBq culture ($n = 56$ aggregates from 5 independent experiments). (**g**) Procedure for ES cell culture combined with FACS sorting and co-culture with mouse rhombic lip-derived cells. FACS-sorted cells were reaggregated on day 13, and dissociated and replated on day 15 along with granule cell precursors from the upper rhombic lip of E15.5 mice. (**h**,**i**) Control culture of rhombic lip-derived cells alone (**h**) or co-culture of rhombic lip-derived cells and FACS-sorted Nephn3-positive ES-derived cells (**i**) on day 25 of co-culture, immunostained with antibody to L7. (**j**–**n**) Co-culture of FACS-sorted Nephn3-positive cells with rhombic lip-derived cells on day 42 (**j**) and day 79 (**k**–**n**), immunostained with antibodies to L7 (**j**) and L7 plus GluRδ2 (**k**–**n**). Arrowheads in **m** indicate an axon. (**o**) Spontaneous synaptic potentials and action potentials. Arrows indicate presumptive excitatory postsynaptic potentials, and arrowheads indicate presumptive inhibitory postsynaptic potentials. (**p**) Spontaneous synaptic currents without (top) and with bicuculline (middle) or bicuculline and CNQX (bottom). Arrows indicate presumptive excitatory postsynaptic currents, and arrowheads indicate presumptive inhibitory postsynaptic currents. (**q**) Spontaneous action potentials without synaptic inputs. (**r**) Evoked excitatory postsynaptic current without or with AP5 or AP5 and CNQX. Each trace is an average of 5 traces. Scale bars: 200 μm (**c**,**d**,**h**,**i**); 25 μm (**j**,**l**); 100 μm (**k**); 2 μm (**n**). Error bars represent s.e.m.

figures (**Fig. 4l**) were predominantly found at or near the apical area. The nuclei of Ki67+ and Ptf1a+ cells were also localized in the inner zone close to the apical cavity (**Fig. 4m–o**). In contrast, most of the Corl2+ nuclei were at least three to four cells away from the apex, and formed an outer zone that surrounded the Ptf1a+ proliferative zone (**Fig. 4p,q**; day 15). These Corl2+ cells were predominantly found in the outer zones of Nephn3+ rosettes (up to 58.8 ± 11.5% cells in the rosettes), but not in those of Nephn3− rosettes (**Supplementary Fig. 4**).

We next performed a birth-dating comparison between the Corl2+ (Purkinje) and Pax2+ (non-Purkinje[30]) cell populations (these markers were mutually exclusive; **Supplementary Fig. 4**) using a pulse exposure to 5-ethynyl-2-deoxyuridine (EdU) (**Supplementary Fig. 4**). The number of Corl2+ cells that incorporated EdU was significantly higher when the aggregates were exposed to EdU on day 13 than on day 15 or 16 (**Fig. 4r** and **Supplementary Fig. 4**). In contrast, the Pax2+ (non-Purkinje) cell populations were more efficiently labeled by EdU on days 15 and 16 than on day 13 (10–17% of Pax2+ cells were mitotic and Ki67+ on day 16, as *in vivo*; **Fig. 4r**, **Supplementary Fig. 4** and data not shown). Most (>90%) of the Nephn3+ neural rosettes on day 13 were E-cadherin+ (**Fig. 4m**), which marks the Purkinje-generating neuroepithelium, but by day 15 the E-cadherin expression in the Nephn3+ neural rosettes had substantially decreased (not shown). These findings are consistent with the *in vivo* neurogenesis, in that Purkinje cells are the first of the cerebellar cortical neurons to exit the cell cycle. These observations suggest that SFEBq/FIC-cultured cells recapitulate not only regional marker expression but also key temporal and spatial aspects of the *in vivo* development of Purkinje cells.

Mature Purkinje cells from purified progenitors

Taking advantage of the cell-surface localization of Nephn3, we next used this early marker to select Purkinje cell progenitors by timed sorting. In fluorescence-activated cell sorting (FACS) analysis, 25–35% of the SFEBq/FIC cells on day 13 were strongly positive for Nephn3 (**Fig. 5a,b**), and the purified Nephn3+ population generated a large number of Corl2+ cells (82.7 ± 8.4% of total cells) in two

days. In contrast, only 3.1 ± 0.8% of the Neph3$^-$ cells became Corl2$^+$ (**Fig. 5c,d**). We next compared the content of Purkinje cell precursors among Neph3$^+$ progenitors sorted on different days in culture. After sorting, the cells were treated with DAPT to inhibit Notch and thereby promote neuronal differentiation, and cultured for two more days. The vast majority of Neph3$^+$ cells sorted on day 13 differentiated into Corl2$^+$ cells (>90%), and a minor population gave rise to Pax2$^+$ neurons (**Fig. 5e**). In contrast, more Neph3$^+$ cells sorted on day 15 differentiated into Pax2$^+$ neurons (27.1 ± 8.2%) than into Corl2$^+$ cells (5.3 ± 2.9%) (**Fig. 5f**; the DAPT treatment caused at least a two-fold increase in the percentage of Pax2$^+$ neurons; data not shown). Thus, in accordance with the birth-dating analysis, isolating the Neph3$^+$ progenitors on day 13 has proven to be an efficient way to enrich for ES cell–derived Purkinje cell progenitors.

In a conventional high-density neuronal culture, the purified Neph3$^+$ cells gradually died, and the surviving neurons failed to express late Purkinje cell markers such as L7 and Calbindin even two weeks later (data not shown). A similar observation was made with Neph3$^+$ cells purified from fetal cerebellar plate tissues[28] (E12.5), presumably because the appropriate trophic microenvironment could not be established in the purified cell population. To circumvent these problems, we co-cultured Neph3$^+$ cells with cerebellar granule cells, which promotes the maturation and survival of Purkinje cells *in vitro*[31] (we avoided DAPT treatment as it attenuated survival in long-term culture). In the presence of granule cells derived from the rhombic lip (**Fig. 5g**), the purified Neph3$^+$ cells survived and generated a large number of L7$^+$ Calbindin$^+$ PV$^+$ neurons (**Fig. 5h,i** and **Supplementary Fig. 5**) with characteristic, highly arborized dendrites (**Fig. 5j**). When cultured alone, the rhombic lip cells produced no L7$^+$ cells (**Fig. 5h**). Moreover, when we used Neph3$^+$ progenitors derived from *Gad67::GFP* (GAD-GFP) ES cells (>90% of these progenitors became GAD-GFP$^+$ after two days of dissociation culture) in the co-cultures, all of the L7$^+$ neurons expressed GFP (**Fig. 5j**; conversely, 38.2 ± 4.3% of the GFP$^+$ cells expressed L7$^+$). Furthermore, when the rhombic lip cells were isolated from GFP-transgenic mouse cerebella, no Corl2$^+$ or L7$^+$ cells generated from nonlabeled ES cells were GFP$^+$ (**Supplementary Fig. 5**), excluding the possibility of differentiation by cell fusion.

After long-term culture, each ES cell–derived Purkinje cell had dendrites with numerous, well-developed spines that expressed the Purkinje cell–specific glutamate receptor subunit GluRδ2 (**Fig. 5k–n**).

To investigate their functional properties, we performed whole-cell patch-clamp recording of the SFEBq/FIC-induced Purkinje cells after their maturation in co-culture with granule cells. Under current clamp, large Purkinje cells showed frequent action potentials (large spikes) and synaptic potentials (**Fig. 5o**). Voltage-clamp recordings (−50 mV; **Fig. 5p**) revealed that the inward currents (red) were CNQX sensitive, showing that they were AMPA receptor–mediated excitatory glutamatergic synaptic currents (generated by granule cell input[32] *in vivo*), whereas the outward currents (blue) were bicuculline sensitive, meaning that they were $GABA_A$ receptor–mediated inhibitory synaptic currents (presumably from other ES cell–derived GABAergic neurons including Purkinje cells). When these synaptic potentials were suppressed with CNQX and bicuculline, we recorded the repetitive firing of spontaneous action potentials (**Fig. 5q**; current clamp). Such intrinsic excitability is a characteristic of dissociated Purkinje cells[33].

Another intriguing characteristic of mature Purkinje cells is that the NMDA-type glutamate receptor makes no significant contribution to their synaptic responses[34], unlike many other neurons. In Mg^{2+}-free external solution, which unmasks synaptic currents mediated by the NMDA receptor (regardless of AMPA receptor activity), the NMDA receptor antagonist D(−)-2-amino-5-phosphonovaleric acid (AP5) did not significantly affect the amplitude or time course of inward synaptic currents (**Fig. 5r**), although these currents were suppressed completely by CNQX with AP5 (**Fig. 5r**) and by CNQX alone (data not shown). These results are consistent with the inward synaptic current of SFEBq/FIC-induced Purkinje cells being mediated predominantly by the AMPA receptor and not the NMDA receptor, again showing similar electrophysiological properties to native Purkinje cells in primary culture.

Orthotopic integration of ES cell–derived Purkinje cells

The postnatal cerebellum consists of the cortex and the DCN (**Supplementary Fig. 6**). The stratified cortex consists of the molecular layer, which contains parallel fibers and Purkinje cell dendrites, the Purkinje cell layer, the granule layer (containing granule cells), and the white matter (**Supplementary Fig. 6**).

For the transplantation study, Neph3$^+$ cells derived from GAD-GFP ES cells were sorted on day13, and then microinjected into the subventricular space of the E15.5 mouse cerebellar plate *in utero* (**Fig. 6a** and **Supplementary Fig. 6**; 10,000 cells per fetus). The majority of grafted GAD-GFP$^+$ neurons found in the host cerebella expressed Calbindin and L7 at 1 and 4 weeks after transplantation (**Fig. 6b–d** and data not shown; for example, 87.3 ± 4.2% of GAD-GFP$^+$ cells were L7$^+$ at the 4-week point; **Fig. 6e**; the ratio of the surviving GFP$^+$ cells per the total injected cells was ~3%; **Supplementary Fig. 6**), indicating that the ES cell–derived purified precursors differentiated into mature Purkinje cells *in vivo*. This was unlikely to be due to fusion with host cells, as we found no GFP labeling in grafted Purkinje cells generated from red fluorescent protein (RFP)-labeled ES cells (not carrying GFP), when we used the L7-GFP mouse as a host (five mice, each containing >200 grafted Purkinje cells; **Supplementary Fig. 6**). Most of the GAD-GFP$^+$ neurons were located in the Purkinje cell layer (**Fig. 6b–d,f**), suggesting that the ES cell–derived Purkinje cell precursors could undergo orthotopic integration.

Most of the integrated grafted Purkinje cells (>90%, 4 weeks after transplantation) showed normal cell polarity, and had well-developed dendrites growing outward in the molecular layer (**Fig. 6d,g**). High-resolution confocal imaging showed that their primary dendrites frequently received multiple VGluT2$^+$ patches (in a string-of-beads appearance; **Fig. 6h,i**), which reflect the presynaptic inputs of the climbing fibers[35]. In addition, in the periphery of the dendrites, the GluRδ2$^+$ spines were closely associated with the localization of cerebellin (Cbln1), which is specifically found at the presynaptic termini of parallel fibers *in vivo*[36,37] (**Fig. 6j–l**). The grafted Purkinje cells had a long axon extending through the granule layer (**Fig. 6g** and **Supplementary Fig. 6**) and white matter toward the DCN (**Supplementary Fig. 6**).

The DCN contains large (magnocellular) projection neurons that express SMI-32 (a glutamatergic marker; **Supplementary Fig. 6**) and small SMI-32$^-$ neurons (arrows in **Supplementary Fig. 6**). The GAD-GFP axonal terminals from the graft-derived L7$^+$ neurons extended to the DCN in 15–45% of the grafted cerebella (**Fig. 6m–o**), where they formed large synaptophysin$^+$ synaptic boutons that were found preferentially on the soma or the proximal dendritic roots of SMI-32$^+$ magnocellular DCN neurons (**Fig. 6m–o**).

This projection of Purkinje cell axons onto the magnocellular DCN somata is characteristic of the normal DCN[38] (**Supplementary Fig. 6**). A quantitative comparison showed that L7 axons from both endogenous and ES cell–derived Purkinje cells terminated

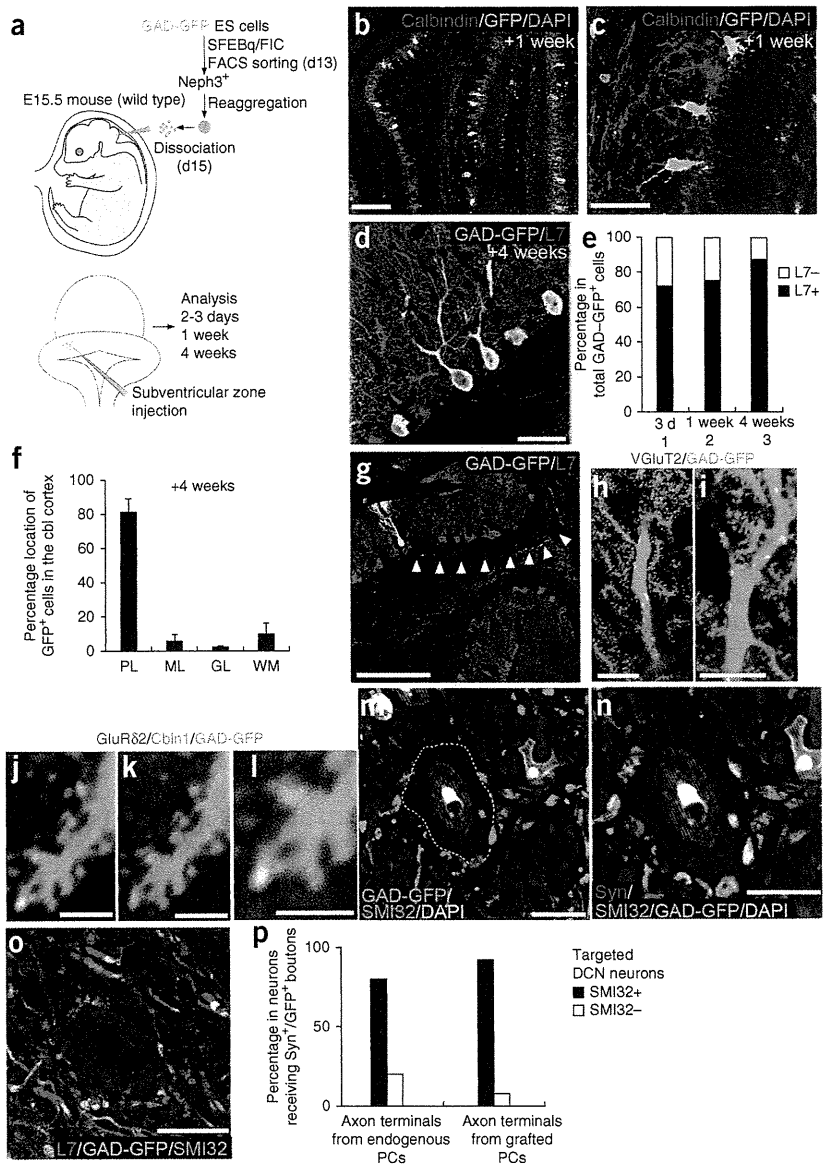

Figure 6 Orthotopic integration of ES cell–derived Purkinje cells into the cerebellum. (**a**) Schematic diagram of the method for *in utero* transplantation. (**b–d**) Integration of multiple grafted GFP$^+$ cells into the Purkinje cell layer of the host cerebellum. Immunostaining showed that grafted GFP$^+$ cells expressed calbindin (**b**,**c**) and L7 (**d**) at 1 week (**b**,**c**) and 4 weeks (**d**) after transplantation. (**e**) Percentage of GAD-GFP$^+$ neurons expressing L7 in the cerebellar plate on the indicated days after transplantation (3 mice each). (**f**) Percentage of integrated GFP$^+$ cells in each layer of the cerebellar cortex (5 mice). (**g**) Integration of a grafted GFP$^+$ cell with proper polarity. The GFP$^+$ axon (arrowheads) extends in the white matter along other L7$^+$ axons. (**h**,**i**) Confocal images of grafted GAD-GFP$^+$ dendrites. Puncta positive for the glutamate transporter VGluT2 were seen along the dendritic shafts of GFP$^+$ neurons (**h**, distal; **i**, proximal portion of dendrite). (**j–l**) High-magnification confocal images of grafted GAD-GFP$^+$ dendritic spines, immunostained for GluRδ2 (**j**), Cbln1 (**k**) and GluRδ2 + Cbln1 (**l**). (**m–o**) Section of an SMI-32$^+$ large glutamatergic DCN neuron. Graft-derived GAD-GFP$^+$ axons terminate at the soma and express synaptophysin (**n**; at their terminal boutons) and L7 (**o**). (**p**) Percentage of neurons surrounded by synaptophysin$^+$ GFP$^+$ boutons in the DCN. The majority of synaptophysin$^+$ L7-GFP$^+$ axons terminated on SMI-32$^+$ large glutamatergic neurons (closed column) in L7-GFP mice (left; 3 mice). Similarly, GAD-GFP$^+$ axons in grafted mice terminated predominantly on SMI-32$^+$ neurons (right; 6 mice). Scale bars: 100 μm (**b**); 50 μm (**c**,**d**); 200 μm (**g**); 10 μm (**h**,**i**,**m–o**); 2.5 μm (**j**,**k**); 2 μm (**l**). Error bars represent s.e.m.

predominantly on magnocellular SMI-32$^+$ DCN neurons, rather than on small SMI-32$^-$ ones (**Fig. 6p**; analysis based on the location of L7$^+$/synaptophysin$^+$ boutons). Together, these findings show that ES cell–derived Purkinje cells can integrate orthotopically, project their axons to the correct DCN targets and form apparently normal synaptic connections *in vivo*.

DISCUSSION

In vitro cerebellar development by self-induction

Making the best use of the emerging knowledge on early cerebellar development[4,5,25,28], we successfully recapitulated the *in vivo* microenvironments of the cerebellum's developmental field in ES cell culture. Our three-step method (**Supplementary Fig. 5**) produced a substantial improvement (up to ~30-fold) over the previously reported frequency of Purkinje cell generation[18–20].

Each specification step is highly efficient and reasonably mimics the *in vivo* developmental process. For instance, >80% of the SFEBq/FI-cultured ES cells expressed En2 in the MHB-region specification step (**Fig. 1h**), and >70% of those were of the isthmus/rhombomere 1 type. Furthermore, 75% of the neuroepithelial rosettes were positive for Neph3$^+$/Ptf1a$^+$ (**Supplementary Fig. 4**). Following FACS sorting, around 90% of the Neph3$^+$ progenitors differentiated into Corl2$^+$ Purkinje cell precursors in 2 days *in vitro* (**Fig. 5e**).

The selective induction of En2$^+$ progenitors (which are present only in a small region of the developing brain *in vivo*) was unexpected, given that it was triggered by only a simple and transient treatment with Fgf2 in the presence of insulin (**Fig. 1i–l**). We infer that this phenomenon reflects a special characteristic of MHB development, involving self-inductive regulation. One reasonable interpretation is that the combination of two weak caudalizing signals (Fgf2 and insulin) was just sufficient to 'prepattern' the aggregates for a broad mid-hindbrain regionalization without interfering with the endogenous self-inductive program mediated by signals from the isthmic organizer. Subsequently, endogenous Wnt1 and Fgf8 signals (and related signals) could have formed a robust self-inductive system that led to MHB development and the concurrent generation of the appropriate cell types for the neighboring tissues (**Supplementary Fig. 1**). The existence of such prepatterning and self-development was also supported by a previous explant study showing that the embryonic neuroectoderm at the mid-streak stage is already prepatterned for tissue-autonomous *En2* expression, far before its onset at the early somite stage[39].

In this view, it is reasonable that the direct application of exogenous Fgf8 and Wnt1, which could perturb their endogenous signaling counterparts, could have resulted in relatively less efficient induction of En2, unlike the simple Fgf2 treatment, which is thought to cause little interference with the subsequent self-inductive processes. The use of chemically defined medium was probably also helpful in this highly selective differentiation, because it avoided undefined factors that could complicate these signaling interactions. Indeed, the addition of KSR (knockout serum replacement), which is commonly used in ES cell culture, reduced the efficiency of En2 induction (data not shown). In addition, selective neural differentiation in SFEBq culture occurs without obvious mesodermal differentiation[21,22] (even in the presence of Fgf); this might also help to simplify the cellular interactions for the self-inductive development of the MHB.

Generally speaking, in the developing brain, the rostral-caudal determination occurs earlier than decisive dorsal-ventral patterning. In our system, the dorsal specification into the cerebellar plate identity was achieved by using the hedgehog inhibitor cyclopamine (**Fig. 2**) from day 7. This method of passive dorsal specification proved to be better for the generation of Purkinje cell progenitors than was active dorsalization using the strong dorsalizing factor BMP4, which preferentially induced the differentiation of glutamatergic Math1$^+$ granule cells and Tbr1$^+$ DCN neurons (**Fig. 2i,m**). This differential effect can be explained, at least in part, by the fact that Purkinje cells arise from a broad area of the dorsal (alar) plate of rhombomere 1, whereas granule cells and DCN neurons originate exclusively from the dorsal-most tip of the neural tube. In accordance with this interpretation, treatment with both cyclopamine and BMP4 was less effective for inducing Purkinje cell progenitors than cyclopamine treatment alone (**Fig. 2v**, lanes 4 and 5).

Remaining questions and future applications

SFEBq/FIC-generated cerebellar progenitors were efficiently isolated by FACS using an anti-Neph3 antibody. The day of culture on which cells were sorted was a key parameter for obtaining Purkinje cell–generating progenitors. Progenitors purified from day 13 in culture (but not day 15 in culture) differentiated into Corl2$^+$ Purkinje cell precursors (postmitotic) at high frequency in dissociation culture (~90%; **Fig. 5d,e**). In contrast, the generation of Pax2$^+$ cells (which generate non-Purkinje GABAergic neurons such as Golgi cells; **Supplementary Fig. 5**) from Neph3$^+$ progenitors was more efficient with cells sorted on day 5 than on day 13. This differential relationship was consistent with our birth-dating analysis (**Fig. 4r**) and the expression profile of E-cadherin (which is expressed more strongly on day 13 than on day 15) as well as with the timing of cerebellar development *in vivo*.

In a co-culture system of sorted Neph3$^+$ progenitors with rhombic lip–derived granule cells, ~40% of the ES cell–derived GABAergic neurons (GAD-GFP$^+$) were L7$^+$ Purkinje cells (**Fig. 5i**). Although this percentage, seen after long-term co-culture (25 d), was fairly remarkable, it was still lower (about by half) than the percentage (83–90%) of Corl2$^+$ precursors generated from Neph3$^+$ progenitors in dissociation culture 2 days after sorting (**Fig. 5d**). This reduced efficiency might reflect the moderate dilution of the Purkinje cell population by non-Purkinje GABAergic neurons that were also generated from Neph3$^+$ progenitors after the Purkinje cell production was finished (also note that a portion of Pax2$^+$ cells are initially mitotic; **Supplementary Fig. 4**). The contribution of biased apoptosis remains elusive, as our preliminary study detected only low percentages of ES cell–derived apoptotic cells (<1% positive for active caspase 3) regardless of L7 expression (not shown).

Purkinje cell loss is associated with cerebellar degeneration, particularly of the SCA6 type[40]. Unfortunately, cell transplantation is hindered by a technical issue: exogenous cerebellar neurons have historically had low integration efficiency. In this study, we injected Neph3$^+$ progenitors into the cerebellar plate of E15.5 mice. Four weeks later, the numbers of surviving grafted GAD-GFP$^+$ neurons was typically ~3% of the grafted neurons, although most (>90%) of the integrated neurons were L7$^+$ Purkinje cells. We also found low integration efficiency in our grafting study of endogenous cerebellar progenitors from GAD-GFP mice (<2–3%; **Supplementary Fig. 6**), indicating that this problem is not limited to the ES cell–derived cells. The integration efficacy was even lower when cells were transplanted into the postnatal cerebellum (postnatal day 3 to week 8; **Supplementary Fig. 6**), consistent with previous studies[41]. In contrast to the fetal transplantation, GAD-GFP$^+$ cells that were injected postnatally did not integrate into the postnatal cerebellar cortex but mostly stayed in the white matter, and did not express L7 or calbindin (**Supplementary Fig. 6**). We have attempted to improve the neuronal integration in the adult mouse by using a cerebellar degeneration model line[42], but so far the integration rate remains low, suggesting that it is not simply due to the lack of a niche or free space. We infer that successful cellular integration during the early period after transplantation is an important decisive factor, as both the number of surviving GAD-GFP$^+$ cells and the percentage of L7$^+$ cells among them were much the same a few days and four weeks after grafting (**Fig. 6e** and **Supplementary Fig. 6**). In the future, intensive efforts to create permissive *in vivo* conditions for the improved survival of grafted cerebellar neurons will be essential for the functional recovery of cerebellar degeneration by cell replacement.

METHODS

Methods and any associated references are available in the online version of the paper at http://www.nature.com/natureneuroscience/.

Note: Supplementary information is available on the Nature Neuroscience website.

ACKNOWLEDGMENTS

We thank H. Enomoto and M. Eiraku for comments, T. Wataya for help in tissue preparation and members of the Sasai laboratory for discussion and advice. This work was supported by grants-in-aid from the Ministry of Education, Culture, Sports, Science and Technology (Japan), the Kobe Cluster Project, the Leading Project (Y.S.) and the National Center of Neurology and Psychiatry (K.M.).

AUTHOR CONTRIBUTIONS

K.M. performed the experiments that comprise the main body of this work. A.N. assisted with cell culture and histology. Y.O. and E.M. contributed to the FACS analysis. H.M. and T.H. performed electrophysiological analysis. S.H. and A.K. contributed to the ataxia model mouse analysis. K.O. and Y.Y. provided GAD-GFP transgenic mice. Y.S. wrote the manuscript and designed the experiments with K.M.

COMPETING FINANCIAL INTERESTS

The authors declare no competing financial interests.

Published online at http://www.nature.com/natureneuroscience/.
Reprints and permissions information is available online at http://www.nature.com/reprintsandpermissions/.

1. Wingate, R.J.T. & Hatten, M.E. The role of the rhombic lip in avian cerebellum development. *Development* **126**, 4395–4404 (1999).
2. Zervas, M., Milet, S., Ahn, S. & Joyner, A.L. Cell behavior and genetic lineage of the mesencephalon and rhombomere 1. *Neuron* **43**, 345–357 (2004).
3. Park, C., Falls, W., Finger, J.H., Longo-Guess, C.M. & Ackerman, S.L. Deletion in Catna 2, encoding alpha N-catenin, causes cerebellar and hippocampal lamination defects and impaired startle modulation. *Nat. Genet.* **31**, 279–284 (2002).
4. Hoshino, M. *et al. Ptf1a*, a HLH transcriptional gene, defines GABAergic neuronal fates in cerebellum. *Neuron* **47**, 201–213 (2005).

5. Machold, R. & Fishell, G. Math1 is expressed in temporally discrete pools of cerebellar rhombic-lip neural progenitors. *Neuron* **48**, 17–24 (2005).
6. Ben-Arie, N. *et al. Math1* is essential for genesis of cerebellar granule neurons. *Nature* **390**, 169–172 (1997).
7. Fink, A.J. *et al.* Development of the deep cerebellar nuclei: transcription factors and cell migration from the rhombic lip. *J. Neurosci.* **26**, 3066–3076 (2006).
8. Joyner, A.L. *Engrailed*, *Wnt* and *Pax* genes regulate midbrain-hindbrain development. *Trends Genet.* **12**, 15–20 (1996).
9. Crossley, P.H., Martinez, S. & Martin, G. Midbrain development induced by FGF8 in the chick embryo. *Nature* **380**, 66–68 (1996).
10. Liu, A., Losos, K. & Joyner, A.L. FGF8 can activate *Gbx2* and transform regions of the rostral mouse into a hindbrain fate. *Development* **126**, 4827–4838 (1999).
11. Martinez, S., Crossley, P.H., Cobos, I., Rubenstein, J.L.R. & Martin, G.R. FGF8 induces formation of an ectopic isthmic organizer and isthmocerebellar development via repressive effect on *Otx2* expression. *Development* **126**, 1189–1200 (1999).
12. Meyers, E.N., Lewandoski, M. & Martin, G.R. An *Fgf8* mutant allelic series generated by Cre- and Flp-mediated recombination. *Nat. Genet.* **18**, 136–141 (1998).
13. Sato, T., Araki, I. & Nakamura, H. Inductive signal and tissue responsiveness defining the tectum and the cerebellum. *Development* **128**, 2461–2469 (2001).
14. Thomas, K.R. & Capecchi, M.R. Targeted disruption of the murine int-1 proto-oncogene resulting in severe abnormalities in midbrain and cerebellar development. *Nature* **346**, 847–850 (1990).
15. McMahon, A.P., Joyner, A.L., Bradley, A. & McMahon, J.A. The midbrain-hindbrain phenotype of *Wnt-1*$^{-}$/*Wnt-1*$^{-}$ mice results from stepwise deletion of *engrailed*-expressing cells by 9.5 days postcitum. *Cell* **69**, 581–595 (1992).
16. Simeone, A. Positioning the isthmic organizer where *Otx2* and *Gbx2* meet. *Trends Genet.* **16**, 237–240 (2000).
17. Watanabe, K. *et al.* Directed differentiation of telencephalic precursors from embryonic stem cells. *Nat. Neurosci.* **8**, 288–296 (2005).
18. Su, H.-L. *et al.* Generation of cerebellar neuron precursors from embryonic stem cells. *Dev. Biol.* **290**, 287–296 (2006).
19. Salero, E. & Hatten, M.E. Differentiation of ES cells into cerebellar neurons. *Proc. Natl. Acad. Sci. USA* **104**, 2997–3002 (2007).
20. Tao, O. *et al.* Efficient generation of mature cerebellar Purkinje cells from mouse embryonic stem cells. *J. Neurosci. Res.* **88**, 234–247 (2010).
21. Wataya, T. *et al.* Minimization of exogenous signals in ES cell culture induces rostral hypothalamic differentiation. *Proc. Natl. Acad. Sci. USA* **105**, 11796–11801 (2008).
22. Eiraku, M. *et al.* Self-organized formation of polarized cortical tissues from ESCs and its active manipulation by extrinsic signals. *Cell Stem Cell* **3**, 519–532 (2008).
23. Davis, C.A. & Joyner, A.L. Expression patterns of the homeo box-containing genes *En-1* and *En-2* and the proto-oncogene *int-1* diverge during mouse development. *Genes Dev.* **2**, 1736–1744 (1988).
24. Ye, W., Shimamura, K., Rubenstein, J.L.R., Hynes, M.A. & Rosenthal, A. Fgf and Shh signals control dopaminergic cell fate in the anterior neural plate. *Cell* **93**, 755–766 (1998).
25. Minaki, Y., Nakatani, T., Mizuhara, E., Inoue, T. & Ono, Y. Identification of a novel transcriptional co-repressor, Corl2, as a cerebellar Purkinje cell–selective marker. *Gene Expr. Patterns* **8**, 418–423 (2008).
26. Alder, J., Lee, K.J., Jessel, T.M. & Hatten, M.E. Generation of cerebellar granule neurons *in vivo* by transplantation of BMP-treated neural progenitor cells. *Nat. Neurosci.* **2**, 535–540 (1999).
27. Wilson, L. & Maden, M. The mechanisms of dorsoventral patterning in the vertebrate neural tube. *Dev. Biol.* **282**, 1–13 (2005).
28. Mizuhara, E. *et al.* Purkinje cells originate from cerebellar ventricular zone progenitors positive for Neph3 and E-cadherin. *Dev. Biol.* **338**, 202–214 (2010).
29. Altman, J. & Bayer, S.A. *Development of the Cerebellar System in Relation to its Evolution, Structures and Functions* (CRC Press, Boca Raton, Florida, 1997).
30. Maricich, S.M. & Herrup, K. Pax2 expression defines a subset of GABAergic interneurons and their precursors in the developing murine cerebellum. *J. Neurobiol.* **41**, 281–294 (1999).
31. Baptista, C.A., Hatten, M.E., Blazeski, R. & Mason, C.A. Cell-cell interactions influence survival and differentiation of purified Purkinje cells *in vitro*. *Neuron* **12**, 243–260 (1994).
32. Hirano, T. & Kasono, K. Spatial distribution of and inhibitory synapses on a Purkinje cell in a rat cerebellar culture. *J. Neurophysiol.* **70**, 1316–1325 (1993).
33. Raman, I.M. & Bean, B.P. Ionic currents underlying spontaneous action potentials in isolated cerebellar Purkinje neurons. *J. Neurosci.* **19**, 1663–1674 (1999).
34. Hirano, T. & Hagiwara, S. Synaptic transmission between rat cerebellar granule and Purkinje cells in dissociated cell culture: effects of excitatory-amino acid transmitter antagonists. *Proc. Natl. Acad. Sci. USA* **85**, 934–938 (1988).
35. Miyazaki, T., Fukaya, M., Shimizu, H. & Watanabe, M. Subtype switching of vesicular glutamate transporters at parallel fibre–Purkinje cell synapses in developing mouse cerebellum. *Eur. J. Neurosci.* **17**, 2563–2572 (2003).
36. Matsuda, K. *et al.* Cbln1 is a ligand for an orphan glutamate receptor delta2, a bidirectional synapses organizer. *Science* **328**, 363–368 (2010).
37. Uemura, T. *et al.* Trans-synaptic interaction of GluRδ2 and Neurexin through Cbln1 mediates synapse formation in the cerebellum. *Cell* **141**, 1068–1079 (2010).
38. Garin, N. & Escher, G. The development of inhibitory synaptic specialization in the mouse deep cerebellar nuclei. *Neuroscience* **105**, 431–441 (2001).
39. Ang, S.L. & Rossant, J. Anterior mesendoderm induces mouse engrailed genes in explant cultures. *Development* **118**, 139–149 (1993).
40. Frontali, M. Spinocerebellar ataxia type 6: Channelopathy or glutamine repeat disorder? *Brain Res. Bull.* **56**, 227–231 (2001).
41. Cendelin, J.I., Korelusova, I. & Vozeh, F. The effect of cerebellar transplantation and enforced physical activity on motor skills and spatial learning in adult lurcher mutant mice. *Cerebellum* **8**, 35–45 (2009).
42. Ikeda, H. *et al.* Expanded polyglutamine in the Machado-Joseph disease protein induces cell death *in vitro* and *in vivo*. *Nat. Genet.* **13**, 196–202 (1996).

ONLINE METHODS

ES cell culture. Mouse ES cells (EB5) were maintained as described[17]. To generate GAD67-GFP knock-in ES cells, we obtained E3.5 blastocysts from pregnant female 129x1/SvJ mice mated with heterozygous GAD67-GFP (neo) mice[43] and subjected them to ES cell derivation on mouse embryonic fibroblasts. For SFEBq culture, ES cells were dissociated to single cells in 0.25% trypsin-EDTA and quickly reaggregated in differentiation medium (3,000 cells per 150 µl per well) in 96-well low-cell-adhesion plates (Lipidure Coat, NOF). The basal differentiation medium used during days 0–11 was gfCDM (modified from ref. 44), consisting of Isocove's modified Dulbecco's medium/Ham's F-12 1:1, chemically defined lipid concentrate, penicillin/streptomycin, monothioglycerol (450µM), apo-transferrin (15 µg ml^{-1}) and crystallization-purified BSA (5 mg ml^{-1}, >99%, Sigma). The medium was supplemented with insulin (7 µg ml^{-1}) on day 0 (the starting day of differentiation culture) unless otherwise noted. Recombinant proteins were purchased from R&D Systems. Cyclopamine was purchased from Toronto Research Chemicals.

Immunohistochemistry. Immunohistochemistry was performed as described[17]. For quantitative analysis, 16–24 aggregates were examined for each experiment, which was repeated at least five times. Antibodies to the following proteins were used at the indicated dilutions: En2 (goat 1:100, Santa Cruz), Otx2 (goat 1:100, Santa Cruz, rabbit 1:100, Abcam), Pax2 (rabbit 1:200, Zymed, mouse 1:1,000, Abnova), Tbr1 (rabbit 1:1,000, Chemicon), 5HT (rabbit 1:1,000, Protos), tyrosine hydroxylase (sheep 1:100, Chemicon), Lhx5 (goat 1:100, Santa Cruz), Calbindin (mouse 1:1,000, Swant, goat 1:100, SantaCruz), Neph3 (Kirrel2) (goat 1:2,000, R&D Systems), E-cadherin (rat 1:50, Takara), N-cadherin (mouse 1:1,000, BD Transduction), Ki67 (mouse 1:200, BD Pharmingen), aPKC (PKCζ, rabbit 1:100, Santa Cruz), pH3 (mouse 1:500, Cell Signaling), GluRδ2 (goat 1:100, Santa Cruz), Synaptophysin (rabbit 1:400, Zymed), SMI-32 (mouse 1:200, Covance), Meis1/2 (goat 1:100, Santa Cruz), Parvalbumin (mouse 1:2,000, Sigma), VGluT2 (guinea pig 1:1,000, Chemicon), Cbln1 (rabbit 1:200, Abcam), Neurogranin (rabbit 1:1,000, Chemicon), Corl2 (ref. 25) (rabbit 1:200), Ptf1a[25] (hamster 1:2), Neph3 (ref. 28) (hamster 1:100), Math1 (ref. 18) (guinea pig 1:3,000), L7 (ref. 18) (rabbit 1:5,000). DAPI was used for counterstaining the nuclei (Molecular Probes). NeuroTrace was used for Nissl's staining (Molecular Probes). NEO-STEM was used for labeling of grafted cells (Biterials). Stained sections were analyzed with LSM710 confocal microscope (Zeiss). Images were assembled by Adobe Photoshop CS2.

Quantitative PCR. Quantitative PCR was performed using the 7500 Fast Real Time PCR System (Applied Biosystems) and data were normalized to GAPDH expression. The primers used for qPCR are listed in **Supplementary Table 1**. The values shown on graphs represent the mean ± s.e.m. For quantitative analysis, 24–48 aggregates were examined for each experiment, which was repeated at least five times.

Neuronal differentiation culture. For the SFEBq/FIC culture, Fgf2 (20 ng ml^{-1}) was added on day 1, and cyclopamine (10µM) on day 7 to the insulin-containing gfCDM medium (**Fig. 3a**). On day 11, the cell aggregates were transferred to a collagen-coated membrane (Transwell-COL, Corning) in DMEM/F12/N2/10%FBS supplemented with 7 g l^{-1} glucose.

FACS sorting. For FACS analysis, cells were counted with FACSAria (Becton Dickinson), and the data were analyzed with the FACSDiva software (Becton Dickinson). The cells were dissociated to single cells by Accumax (Chemicon) treatment and analyzed at 4 °C. For the Neph3$^+$ cell isolation experiments, the cells were dissociated with Accumax on day 13 or day 15 and filtered through a Cell Strainer (BD Biosciences). The cells were then incubated with an anti-Neph3 monoclonal antibody and labeled with a PE-conjugated secondary antibody (BD Biosciences). Sorted cells were collected in ice-cold DMEM/F12/N2/10%FCS and quickly reaggregated in low-cell-adhesion 96-well culture plates (1 × 10^4 cells per well). Sorted Neph3-positive and -negative cells were reanalyzed by FACS and qPCR to confirm the quality of sorting. For forced neuronal differentiation, DAPT (10 µM) was added after the sorting.

Birth-dating analysis. For the *in vitro* birth-dating analysis, aggregates were treated with EdU (5 µg ml^{-1}, Invitrogen) on days 10, 11, 12, 13, 14, 15 or 16, and rinsed with medium after 12 h, to remove the EdU. On day 19, the cell aggregates were fixed and cryosectioned. Sections were immunostained for EdU and each cerebellar neuron marker. The percentage of EdU$^+$ cells that expressed Corl2 or Pax2 was quantified. For the quantification, 16–24 aggregates were examined for each experiment, which was repeated at least three times.

Dissociation neuronal coculture. For cocultures of granule cells with cerebellar Purkinje cells, the upper rhombic lip (rhombomere 1) was strictly dissected from E15.5 mice and dissociated with Accumax. The cells were sorted on day 13 *in vitro*, reaggregated, and the reaggregated Neph3$^+$ cells were dissociated again on day 15 (2 days after the sorting). The sorted cells were mixed with the dissociated mice rhombic lip cells at a ratio of 1:3, and the mixed cells were plated onto poly-D-lysine/laminin-coated cover glasses at a density of 2 × 10^5 cells per 100 µl per cm^2 in DMEM/F12/N2/10%FBS/penicillin-streptomycin. After a 3-h incubation in a CO_2 incubator, culture medium was added to each dish to reduce the concentration of serum. The culture medium consisted of DMEM/F12/N2 supplemented with tri-iodothyronine (T3, 0.5 ng ml^{-1}). The cells were fed once a week by replacing half of the old medium with fresh medium that was supplemented with BSA (100 µg ml^{-1}) and cytosine arabinoside (Ara-C, 4 µM)[45].

Electrophysiological analysis. Electrophysiological analysis was performed as described[34]. Whole-cell patch-clamp recordings were made from dissociated cultured cells at room temperature (~21–25 °C). The extracellular bath solution consisted of (mM): 145 NaCl, 5 KOH, 2 $CaCl_2$, 1 $MgCl_2$, 10 HEPES and 10 glucose (pH 7.3). The patch pipette solution consisted of (mM): 140 D-glucuronic acid, 7 KCl, 155 KOH, 5 EGTA, 10 HEPES, 2 Mg-ATP and 0.2 Na-GTP. The membrane potential was held at −70 mV unless otherwise stated. The junction potential was offset. The signal was filtered at 2.9 kHz and digitized at 20 kHz. Only recordings with an input resistance of more than 100 MΩ and a series resistance of <25 MΩ were accepted. In some experiments, bicuculline (20 µM) or CNQX (10 µM) was applied to the bath solution. To record evoked EPSCs, a voltage pulse (10 V, 2 ms) was applied to the soma of a granule cell through a glass electrode in a bath solution lacking Mg^{2+} and including 1 µM glycine. In this experiment, QX-314 (5 mM) was added to the internal solution to block action potentials. AP5 (100 µM) and CNQX were used to suppress AMPA-type and NMDA-type glutamate receptor–mediated currents, respectively. When synaptic potentials were suppressed, the resting membrane potential of the ES cell–derived Purkinje cells was −57.5 ± 3.0 mV, and the amplitude, half-height width and frequency of the action potentials were 52.4 ± 7.9 mV, 1.8 ± 0.8 ms and 8.4 ± 4.5 Hz, respectively.

***In utero* injection.** The transplanted cells were *GAD67-GFP* ES cells that were prepared by FACS sorting on day 13. The Neph3$^+$ cells were aggregated *in vitro* for 2 days, and then dispersed with Accumax (no DAPT treatment was given, as it was less beneficial for long-term survival). To perform the transplantation, pregnant mice (on day 15.5 of gestation; the cerebellar anlage at this stage contained 8.2–9.1 × 10^4 cells, and 1.8–2.0 × 10^4 of these cells were Neph3$^+$ by flow cytometry) were deeply anesthetized with an intraperitoneal injection of sodium pentobarbital. The uterine horns were exposed, and 2 µl of cell suspension (5 × 10^3 cells per µl) was injected into the cerebellar plate and throughout the fourth ventricle of each embryo with a glass micropipette. The cerebellum was dissected at indicated time-points, sectioned at a 50-µm thickness, and the sections were immunostained.

Mice. Female 129x1/SvJ mice, pregnant C57BL/6-Tg(CAG-EGFP) mice, C57BL/6 and ICR mice were purchased from Nihon-SLC. B6;FVB-Tg(Pcp2-EGFP)2Yuza/J mice (described as L7-GFP mice) were obtained from Jackson Laboratory[46].

43. Tamamaki, N. *et al.* Green fluorescent protein expression and colocalization with carletinin, parvalbumin, and somatostatin in the GAD67-GFP knock-in mice. *J. Comp. Neurol.* **467**, 60–79 (2003).
44. Johansson, B.M. & Wiles, M.V. Evidence of involvement of activin A and bone morphogenetic protein 4 in mammalian mesoderm and hematopoietic development. *Mol. Cell. Biol.* **15**, 141–151 (1995).
45. Tabata, T. *et al.* A reliable method for dissociated mouse cerebellar cells enriched for Purkinje neurons. *J. Neurosci. Methods* **104**, 45–53 (2000).
46. Tomomura, M., Rice, D.S., Morgan, J.I. & Yuzaki, M. Purification of Purkinje cells by fluorescence-activated cell sorting from transgenic mice that express green fluorescent protein. *Eur. J. Neurosci.* **14**, 57–63 (2001).

Interaction of ataxin-3 with huntingtin-associated protein 1 through Josephin domain

Yukio Takeshita[a,b], Ryutaro Fujinaga[a], Keiji Kokubu[a], Md. Nabiul Islam[a], Mir Rubayet Jahan[a], Akie Yanai[a], Akira Kakizuka[c] and Koh Shinoda[a]

Huntingtin-associated protein 1 (HAP1) is an essential component of the stigmoid body (STB) and known as a possible neuroprotective interactor with causative proteins for Huntington's disease, spinal and bulbar muscular atrophy, spinocerebellar ataxia type 17 (SCA17), and Joubert syndrome. To clarify what other causative molecules HAP1/STB could interact with, we cloned normal causative genes for several neural disorders from human brain RNA library and evaluated their subcellular interaction with HAP1/STB by immunocytochemistry and immunoprecipitation after cotransfection into Neuro2a cells. The results clearly showed that HAP1/STB interacts with the normal ataxin-3 through Josephin domain and polyglutamine-expanded mutants derived from SCA3 as well. The findings suggest that HAP1/STB could modify the physiological function of normal ataxin-3 and pathogenesis of SCA3 attributable to the mutant ataxin-3. *NeuroReport* **22:232–238 © 2011 Wolters Kluwer Health | Lippincott Williams & Wilkins.**

NeuroReport 2011, 22:232–238

Keywords: Machado-Joseph disease, Huntington's disease, Triplet Repeat, Neurode generation, spinocerebellar ataxia type 3, stigmoid body

[a]Department of Neuroscience, Yamaguchi Graduate University School of Medicine, Ube, Yamaguchi, Japan, [b]The Japan Society for the Promotion of science, Tokyo and [c]Laboratory of Functional Biology, Graduate School of Biostudies, Kyoto University, Kyoto, Japan

Correspondence to Dr Koh Shinoda, Department of Neuroscience, Yamaguchi University School of Medicine, 1-1-1 Minami-Kogushi, Ube, Yamaguchi 755-8505, Japan
Tel: +81 836 22 2204; fax: +81 836 22 2205;
e-mail: shinoda@yamaguchi-u.ac.jp

Received 14 December 2010 **accepted** 24 January 2011

Introduction

The stigmoid body (STB) was first identified as a distinct, spherical-to-ovoidal, nonmembrane-bound inclusion (0.5–3 μm in diameter) in the cytoplasm of neurons in the limbic and the hypothalamus of healthy rats [1–3]. The STB has none of the aggresomal characteristics, such as being ubiquitinated and surrounded by vimentin, indicating that the STB is a physiological entity distinct from pathological aggresome [4]. Huntingtin-associated protein 1 (HAP1) induces the formation of STB by its complementary DNA (cDNA) transfection into HEK293 cells [5] and it is detected in the STB of the rat brain [6]. In the mouse brain, the STB and HAP1 messenger RNA have a similar distribution [7] and the STB formation is suppressed in the brain of *Hap1* (+/−) mice [8]. This evidence has led to the suggestion that HAP1 is an essential component, hence a marker, of STBs [3].

HAP1 interacts with huntingtin in polyglutamine(polyQ)-dependent manner [9] and has a protective effect on neurons against apoptosis induced by polyQ-expanded huntingtin [7,8]. HAP1/STB also interacts with polyQ-expanded androgen receptor (AR) in polyQ-dependent manner through a ligand-binding domain, and it suppresses apoptosis induced by a polyQ-expanded AR derived from spinal and bulbar muscular atrophy (SBMA) [10]. In addition, HAP1/STB is associated with TATA-binding protein [11], the polyQ-expansion of which causes spinocerebellar ataxia type 17 (SCA17), and Abelson helper integration site 1 [12], mutations of which are linked to nontriplet neuropsychiatric diseases including Joubert syndrome and schizophrenia [13]. The line of data suggests that HAP1/STB could play a protective role in Huntington's disease, SBMA, SCA17, and Joubert syndrome, leading to the 'HAP1/STB protection hypothesis' that HAP1/STB expression raises the threshold of vulnerability for neurodegeneration and renders more beneficial stability to neurons with HAP1/STB than without it [7]. It remains to be determined, however, how far the hypothesis can be applied to other neural disorders.

In this study, to screen what other neural-disorder-related molecules are possibly involved in the interaction with HAP1/STBs, we cloned causative molecules in several representative neural disorders from normal human brain RNA library and evaluated their subcellular interaction with HAP1/STB in Neuro2a cells.

Methods

Plasmids and Cell culture

Plasmids used here were PCR-amplified using the primers listed in Supplementary Table 1 (Supplemental digital content 1 *http://links.lww.com/WNR/A106*). As target molecules, we choose amyloid precursor protein (APP) in Alzheimer-type dementia, α-synuclein, ubiquitin carboxy-terminal esterase L1 (UCH-L1) in Parkinson's disease, transactive

Supplemental digital content is available for this article. Direct URL citations appear in the printed text and are provided in the HTML and PDF versions of this article on the journal's Website (*www.neuroreport.com*).

DOI: 10.1097/WNR.0b013e32834505f4

response DNA-binding protein of 43 kDa (TDP-43) in amyotrophic lateral sclerosis, ataxin-1 in SCA1, ataxin-3 in SCA3, and monoamine oxidase A (MAO-A) in schizophrenia. HAP1 cDNA obtained from Full-length Human Clone Collection (Invitrogen, Carlsbad, California, USA) were cloned into the *Eco*RI-*Xho*I-digested pcDNA3 vector (Invitrogen). The isolation of ataxin-3Q27 and ataxin-3Q79 cDNAs has been described earlier [14] and was used to reconstruct FLAG-tagged ataxin-3Q27 and ataxin-3Q79 using Gateway technology (Clontech, Mountain View, California, USA). Ataxin-3 deletion mutants were amplified from cDNA encoding ataxin-3 by PCR. The cDNAs of the other target molecules were obtained from human brain total RNA (Clontech) by reverse transcriptase-PCR and were used to construct p3 × FLAG-CMV-10 vector (SIGMA, St Louis, Missouri, USA) using Gateway technology. The plasmids cloned in this study were verified by sequencing. The mouse neuroblastoma (Neuro2a) cell culture was done as described earlier [10].

Western blot analysis, fluorescence immunocytochemistry, cell count, and statistical analysis

Western blot analysis and immunocytochemistry with rabbit anti-HAP1 polyclonal antibody (HAP1 H-300, Santa Cruz Biotechnology, Santa Cruz, California, USA) and mouse anti-FLAG monoclonal antibody (FLAG-M5, Sigma-Aldrich, Tokyo, Japan) was performed as described earlier [3,10]. Image analysis, cell count, and statistical analysis was performed as described earlier [10].

Immunoprecipitation and quantitative analysis

Immunoprecipitation was performed using the FLAG Immunoprecipitation kit (Sigma-Aldrich) according to the manufacturer's instructions. Quantitative analysis was performed as described earlier [10].

Results

The expression vectors of HAP1 and FLAG-tagged ataxin-1, ataxin-3Q27, α-synuclein, UCH-L1, APP, TDP-43, and MAO-A were constructed and singly transfected. Western blot analysis of these transfected cell lysates showed distinct bands corresponding to their expected molecular weights (Fig. 1a and b). Most of the cultured cells transfected with HAP1 were observed to form HAP1-immunoreactive solitary inclusions in cytoplasm (HAP1/STBs) as reported earlier [4,5,7] (see Figure 1a Supplemental digital content 2 *http://links.lww.com/WNR/A107*). Immunofluorescence cytochemistry showed that ataxin-1 or TDP-43 was localized mainly in the nucleus (see Figures 1b and f Supplemental digital content 2 *http://links.lww.com/WNR/A107*), whereas ataxin-3Q27, APP, or MAO-A was expressed mainly in the cytoplasm (Fig. 1c, see Figures 1e and g Supplemental digital content 2 *http://links.lww.com/WNR/A107*). UCH-L1 and α-synuclein showed diffused expression in both nucleus and cytoplasm (see Figures 1c and d Supplemental digital content 2 *http://links.lww.com/WNR/A107*).

To evaluate the intracellular relationship between HAP1 and the abovementioned target molecules, the expression vectors of HAP1 and each causative molecule were cotransfected. Cotransfection of expression vectors of HAP1 and ataxin-3Q27 induced distinct cytoplasmic aggregations that were HAP1/ataxin-3 double positive (Fig. 1g–i). In contrast, the other molecules did not interact with HAP1-immunoreactive inclusions (Fig. 1d–f and j–x) and their intracellular localizations in single transfection were unchanged even after cotransfection with HAP1/STB.

To determine the region of ataxin-3 crucial for interaction with HAP1, the expression vectors of three kinds of ataxin-3-deletion mutants were created (Fig. 2a). They included cDNAs encoding Josephin domain (ATX3 1-510), ataxin-3 lacking Josephin domain (ATX3Q27 511-1083), and ataxin-3 lacking Josephin domain and ubiquitin-interacting motifs (ATX3Q27 781-1083). In western blots, cell lysates from the transfected cells showed the expected molecular weights of all these mutants (Fig. 2b). Immunofluorescence cytochemistry showed that a single transfection of ATX3Q27 511-1083 or ATX3Q27 781-1083 resulted in entirely diffused expression (Fig. 2c and d), whereas ATX3 1-510 was expressed ambiguously in nucleus and part of the cytoplasm (Fig. 2e).

Cotransfections of the expression vectors of ATX3 1-510 and HAP1 induced the formation of prominent HAP1/ATX3 1-510 double-labeled cytoplasmic aggregations (Fig. 2l–n). In contrast, cotransfection of HAP1 and ATX3Q27 511-1083 or 781-1083 did not result in HAP1 double-labeled cytoplasmic aggregations (Fig. 2f–k). Then, the coimmunoprecipitation experiment was carried out to biochemically investigate the interaction of the HAP1/STB and ataxin-3Q27 or Josephin domain (Fig. 2o and p). In cells coexpressing HAP1 and ataxin-3Q27 or ATX3 1-510, HAP1 coprecipitated with ataxin-3Q27 and ATX3 1-510. However, HAP1 did not coprecipitate with ATX3Q27 511-1083. The results clearly show that the Josephin domain itself is an essential region for association with HAP1/STB.

A FLAG-tagged-ataxin-3 (ataxin-3Q79) was created (Fig. 3a). In western blots, cell lysates from the transfected cells showed the expected molecular weights (Fig. 3b). Most of the cells were observed to express ataxin-3Q79 diffusely in the nuclei and cytoplasm in fluorescence microscopy (Fig. 3c). Immunofluorescence cytochemistry showed that the HAP1/ataxin-3 double-labeled cytoplasmic-aggregation (Fig. 3d–f). To clarify the difference in the frequency or strength of association with HAP1 between ataxin-3Q27 and ataxin-3Q79, the HAP1/ataxin-3 double-labeled cytoplasmic aggregation formation (HA3-CAF) ratios (HA3-CAF cell number/total cotransfected cell

Fig. 1

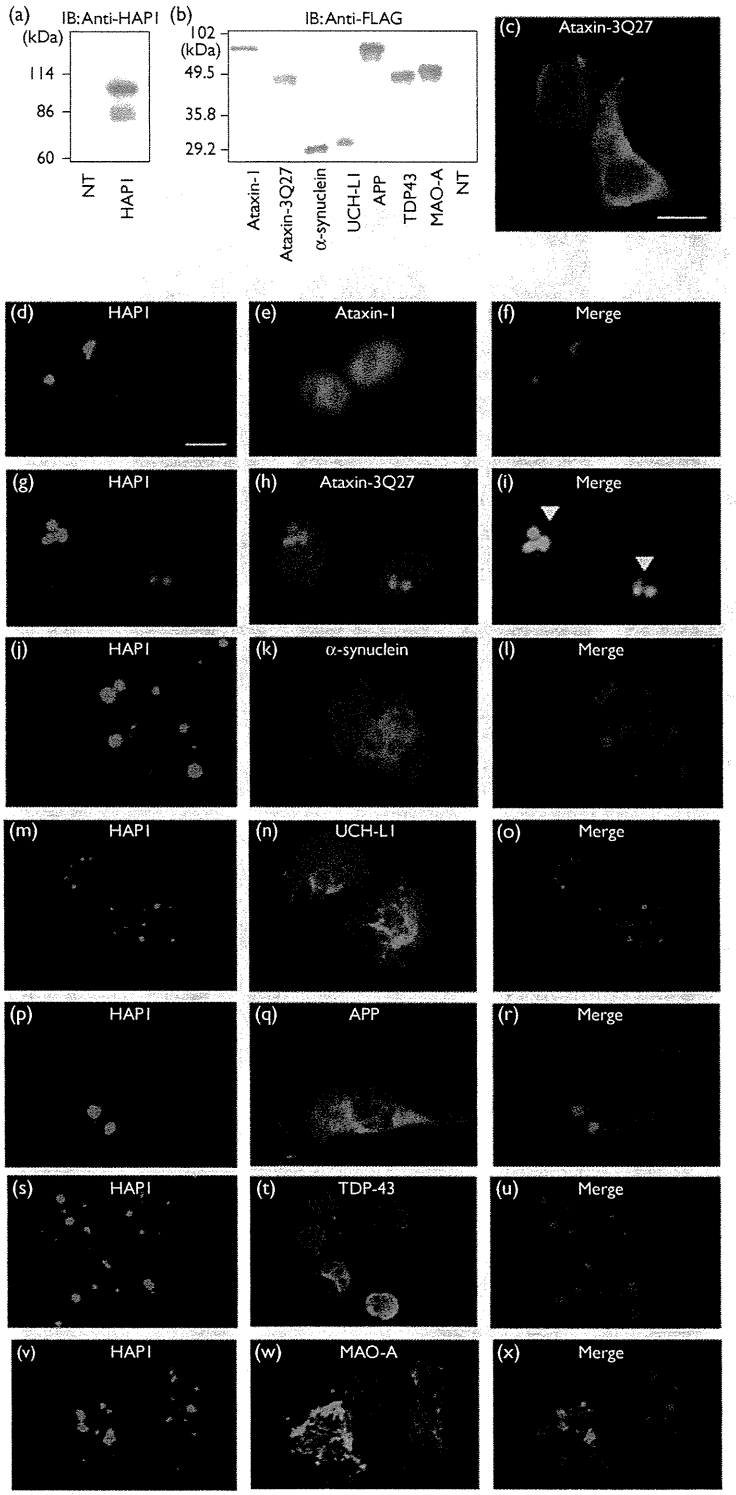

Cotransfection of huntingtin-associated protein 1 (HAP1) and target molecules. (a and b) Western blots for nontransfected (NT) cells and cells transfected with HAP1 (a) and FLAG-tagged target molecules including ataxin-1, ataxin-3Q27, α-synuclein, ubiquitin carboxy-terminal esterase L1 (UCH-L1), amyloid precursor protein (APP), transactive response DNA-binding protein of 43 kDa (TDP-43), and monoamine oxidase A (MAO-A) (b). Molecular weights (kDa) are indicated on the left side. (c) Fluorescence immunocytochemistry for ataxin-3Q27-transfected cells. (d–x) Fluorescence microscopic images of cells cotransfected with HAP1 (Alexa488: green) and target molecules (Alexa594: red). Arrowheads indicate ataxin-3Q27 was associated with HAP1/stigmoid body (f) (bar=10 μm).